Journal of Applied Physics

The native and metastable defects and their joint density of states in hydrogenated amorphous silicon obtained from the improved dual beam photoconductivity method

Cite as: J. Appl. Phys. **133**, 125702 (2023); https://doi.org/10.1063/5.0138257
Submitted: 09 December 2022 • Accepted: 08 March 2023 • Published Online: 24 March 2023

Mehmet Güneş, Jimmy Melskens and Arno H. M. Smets

AIP Publishing

Journal of Applied Physics ARTICLE scitation.org/journal/jap

The native and metastable defects and their joint density of states in hydrogenated amorphous silicon obtained from the improved dual beam photoconductivity method

Cite as: J. Appl. Phys. **133**, 125702 (2023); doi: 10.1063/5.0138257
Submitted: 9 December 2022 · Accepted: 8 March 2023 ·
Published Online: 24 March 2023

Mehmet Güneş,[1,a)] Jimmy Melskens,[2,b)] and Arno H. M. Smets[3,c)]

AFFILIATIONS

[1]Faculty of Sciences, Department of Physics, Mugla Sitki Kocman University, Kotekli Yerleskesi, Mugla, Türkiye
[2]HyET Solar B.V., Westervoortsedijk 71K, 6827 AV Arnhem, The Netherlands
[3]Photovoltaic Materials and Devices, Faculty of Electrical Engineering, Delft University of Technology, Mekelweg 4, 2628 CD Delft, The Netherlands

[a)]**Author to whom correspondence should be addressed:** gunesmehmet1@gmail.com
[b)]jimmy.melskens@hyetsolar.com
[c)]a.h.m.smets@tudelft.nl

ABSTRACT

In this study, undoped hydrogenated amorphous silicon (a-Si:H) thin films deposited under moderate dilution ratios of silane by radio frequency plasma-enhanced chemical vapor deposition (RF-PECVD) have been investigated using steady-state photoconductivity and improved dual beam photoconductivity (DBP) methods to identify changes in multiple gap states in annealed and light-soaked states. Four different gap states were identified in annealed state named as A, B, C, and X states. The peak energy positions of these Gaussian distributions are consistent with those recently identified by Fourier transform photocurrent spectroscopy (FTPS). After *in situ* light soaking, their density increases with different rates as peak energy positions and half-widths remain unaffected. The electron-occupied A and B states located below the dark Fermi level and their density and ratios in the annealed and light-soaked states correlate well with those defects detected by time-domain pulsed electron paramagnetic resonance (EPR) experiments. The A, B, and X states located closer to the middle of the bandgap anneal out at room temperature in dark and define the "fast" states. However, the C states show no sign of room temperature annealing such that they must define the "slow" states in undoped a-Si:H. The results found in this study indicate that the anisotropic disordered network is a more appropriate model than previously proposed defect models based on the continuous random network to define the nanostructure of undoped a-Si:H, where multiple defects, D^0 and non-D^0 defects, can be identified by using the improved DBP method.

I. INTRODUCTION

The Staebler–Wronski effect (SWE)[1] in hydrogenated amorphous silicon, discovered in 1977, was initially attributed to the creation of isolated silicon dangling bonds supported by early electron spin resonance experiments.[2,3] Even though a large number of investigations have been carried out on the SWE and several defect models[4–7] were established in an attempt to explain it, we do not have a complete understanding of its exact origin yet. Such defect models[4–7] were based on the so-called continuous random network, where isolated silicon dangling bonds are the main defects in the nanostructure of a-Si:H. However, more experimental evidence provided by Fourier transform infrared (FTIR) spectroscopy,[8–11] Doppler broadening positron annihilation spectroscopy (DB-PAS),[11–13] and Fourier transform photocurrent spectroscopy (FTPS)[14,15] indicate that a better description of the nanostructure of dense a-Si:H is an anisotropic disordered network, in which isolated silicon dangling bonds and open

volume deficiencies such as divacancies are randomly distributed.[10] In the anisotropic disordered network, not completely hydrogenated divacancies can lead to multiple defects in the nanostructure of a-Si:H with different charged states, which was proposed as an alternative approach to explain the Staebler–Wronski effect.[10] A strong interconnection between these open volume deficiencies and the Staebler–Wronski effect has also been reported by DB-PAS and FTPS experiments.[11,14] Furthermore, time-domain pulsed electron paramagnetic resonance (EPR) experiments[16,17] have recently identified two different paramagnetic silicon dangling bond defects, D^o states, with different origins. The first one, called Type I, is due to paramagnetic silicon dangling bonds located on the inner surface of the voids and the second one, called Type II, corresponds to isolated silicon dangling bonds distributed randomly in the continuous random network. Both types of paramagnetic defect states were shown to play a major role in the Staebler–Wronski effect.[16,17] In addition to these two different paramagnetic defects, detected by the time-domain pulsed EPR experiments, clear experimental evidence has been reported for the creation of non-D^o defects as well.[18–20] These light-induced defects were also classified as "fast" and "slow" states of which the annealing of the "fast" states takes place right after termination of light soaking even at room temperature,[21–25] causing a significant room temperature recovery of the photoconductivity in films as well as in dark forward-biased current–voltage characteristics of p-i-n solar cells.[26] Additionally, it is worth noting here that very short time scale (ms-s) changes in the surface passivation quality of a-Si:H on crystalline wafers have also been reported and differently for different a-Si:H nanostructures,[27] further suggesting that there are "fast" states that should be part of a complete description of the SWE. Moreover, the conventional dual beam photoconductivity (DBP) method that was used to indirectly obtain the sub-bandgap absorption coefficient spectrum has also identified three different gap states below the Fermi level in both annealed and light-soaked states.[18,28,29] Finally, FTPS has also detected four different Gaussian-type midgap states located below the dark Fermi level in a-Si:H thin films as well as in p-i-n solar cells.[14,15] Overall, extensive experimental evidence has accumulated that multiple defect states exist in the nanostructure of undoped a-Si:H.

These defect states (D^o and non-D^o defects) located in the bandgap of undoped a-Si:H are detected by photoconductive sub-bandgap absorption measurements.[30,31] The optical absorption coefficient spectrum, $\alpha(h\nu)$, measured experimentally is determined by the density and distribution of electron-occupied initial states as well as empty final states as defined by the joint density of states function, $J_{DOS}(h\nu)$.[32] It was shown that $J_{DOS}(h\nu)$ at the higher energy region called $J_{EE}(h\nu)$ is totally determined by optical transitions from electron-occupied parabolic valence band extended states to unoccupied parabolic conduction band extended states.[33–35] Below the bandgap energy, $J_{DOS}(h\nu)$ is due to optical transitions from electron-occupied localized defect states to empty conduction band extended states.[33–35] The parabolic extended states and the exponential valence band tails with a characteristic slope of E_{ov} have been extensively used to model the optical transitions and to calculate the $J_{DOS}(h\nu)$ function and applied to the analysis of optical absorption data available for undoped a-Si:H.[34–36] The $J_{DOS}(h\nu)$ function corresponding to optical transitions from occupied midgap states localized in the bandgap is sample dependent due to changes in density and distributions of the midgap states caused by differences in deposition conditions, the light-induced defect creation as well as the annealing of metastability. The first experimental joint density of state spectrum was reported for an n-type doped a-Si:H film by Jackson *et al.* by using the energy-dependent refractive index spectrum as well as the $\alpha(h\nu)$ spectrum measured by spectroscopic ellipsometry and DBP.[32]

In the present work, we have extended our investigation to undoped a-Si:H films deposited at different H_2/SiH_4 dilution ratios with a dense nanostructure by using a new approach of the improved DBP method to identify multiple defect states in annealed and light-soaked states of undoped a-Si:H. In the improved DBP method, the fringe-free absolute $\alpha(h\nu)$ spectrum is independently calculated by using ac photoconductivity and the optical transmission spectrum of the sample without using any normalization or modeling-based fringe removing procedures as required in the conventional DBP method.[31] The validity and accuracy of the calculated $\alpha(h\nu)$ spectrum were compared with an independently measured $\alpha(h\nu)$ spectrum obtained by FTPS for the same a-Si:H film. Then, the $\alpha(h\nu)$ spectrum corresponding to the lowest dc bias light (named as dc bias light-low1) DBP measurement was used to calculate energy-dependent electron-occupied gap states, $kN_{gap}(h\nu)$, to identify the native and light-induced metastable defects located below the dark Fermi level. In addition, the joint density of states function for the DBP spectrum, $J_{DBP}(h\nu)$, as well as that for the FTPS spectrum, $J_{FTPS}(h\nu)$, were calculated by using the corresponding experimental $\alpha(h\nu)$ spectra and the refractive index spectrum provided in the literature[36,37] and compared with $J_{EE}(h\nu)$ calculated for the characteristic parabolic extended states by using the Cody gap, E_{CD}, and $(N_{co}N_{vo})$ product obtained for the sample. A good agreement was obtained between $J_{EE}(h\nu)$ and $J_{DBP}(h\nu)$ functions around the bandgap energy, allowing us a reliable identification of density and energy distributions of multiple defect states in the bandgap of undoped a-Si:H, which can be achieved by the improved DBP method.

Furthermore, the kinetics of light-induced defect creation in the undoped a-Si:H film under AM1.5 white light were investigated at a constant sample temperature of 20 °C in high vacuum by recording real-time photoconductivity changes as well as the sample temperature during light soaking. DBP under dc bias light-low1 and σ_{photo} as a function of light intensity of red light was measured right after light soaking (within 30 min) in order to minimize the effects of room temperature annealing of light-induced defects created by light soaking. In addition, room temperature annealing of the light-induced defects was also investigated by re-characterizing the light-soaked state of the sample a week after light soaking ended as the sample was left in vacuum and in the dark.

This paper is arranged in the following sections. After the Introduction section, experimental details of sample preparation and characterization methods used in the study are given in Sec. II. The derivation of the joint density of states function and density of electron-occupied gap states from the experimental optical absorption coefficient spectrum is explained in Sec. III by using the methods of the theoretical analysis reported in the literature. In Sec. IV, identification of native defect states present in the annealed

state of undoped a-Si:H is established. The Staebler–Wronski defects created by light soaking in the gap of undoped a-Si:H and their kinetics are given in Secs. V and VI, respectively. In Sec. VII, identification of fast and slow states is carried out using room temperature annealing of the Staebler–Wronski defects as detected from σ_{photo} and $\alpha(h\nu)$ spectra. Finally, discussion and conclusions about findings are presented in Sec. VIII.

II. EXPERIMENTAL DETAILS

Undoped hydrogenated amorphous silicon thin films with dense nanostructures were deposited by radio frequency plasma-enhanced chemical vapor deposition (RF-PECVD) at a gas flow rate dilution ratio of R = 7.5 ($R = H_2/SiH_4$) on glass substrates at Delft University of Technology. Special embedded contacts shown in the inset of Fig. 1 are prepared on the glass substrate before deposition of undoped a-Si:H films using a detailed photolithography process to be less sensitive to surface defects and more sensitive to bulk defects in the a-Si:H film. The improved dual beam photoconductivity method was used to measure the relative ac photoconductivity spectrum as the energy of the monochromatic light changes from 0.66 to 2.2 eV. Red dc bias light having a much higher intensity than the monochromatic ac light was used to keep the dc photoconductivity constant during the measurement. The DBP spectrum equivalent to that of the constant photocurrent method (CPM)[30] was measured under the lowest dc bias light intensity with a dc light flux of $6–8 \times 10^{12}\,cm^{-2}\,s^{-1}$ and used to compare the changes in defect distributions after annealing and light soaking. For the lowest dc bias light DBP measurement, the dc/ac ratio of the DBP signal was maintained to be larger than 10 for energies below 1.4 eV, where the occupied gap states below the Fermi level dominate the measured spectrum. In the improved DBP method, the optical transmission spectrum of the sample was simultaneously measured by using a pyroelectric detector placed just behind the sample, which was not considered in the conventional DBP method used by Wronski's group.[31] The DBP yield, $Y_{DBP}(h\nu) = I_{photo}(ac)(h\nu)/flux(h\nu)$, and optical transmission spectra of the sample that have interference fringes were first placed in the absolute scale and then used to calculate the fringe-free absorption coefficient spectrum, $\alpha(h\nu)$, by using Ritter–Weiser optical equations.[38] Self-consistency and accuracy of the calculated $\alpha(h\nu)$ spectrum obtained from the improved DBP method were also compared by using the $\alpha(h\nu)$ spectrum of the same a-Si:H film independently obtained from the Fourier transform photocurrent spectroscopy (FTPS) method. Steady-state photoconductivity, σ_{photo}, was measured using the collimated red light of a He–Ne laser. The flux was measured using a calibrated silicon p-i-n photodiode. Annealing was carried out at 423 K in high vacuum and in the dark for more than 24 h until reproducible annealed state characteristics were obtained. Single-step *in situ* light soaking was applied under white light calibrated to the AM1.5 intensity of an ELH bulb at a constant temperature of 20 °C. Time-dependent photoconductivity was recorded during light soaking under AM1.5 white light. A water filter was used to cut the IR component of white light to prevent heating of the sample during light soaking. In order to prevent the effects of room temperature annealing of light-induced defects[20–22,24] created by AM1.5 white light, the steady-state photoconductivity was measured within 5 min right after light soaking and the lowest dc bias light DBP spectrum (dc bias light-low1) was recorded within a period of 30 min right after light soaking ended. All measurements of DBP and σ_{photo} were performed in a high vacuum of $2–3 \times 10^{-6}$ mbar and at 300 K. A dc voltage in the Ohmic region of contacts was applied to measure both dc and ac photoconductivities of the sample.

III. JOINT DENSITY OF STATES FUNCTION AND ELECTRON-OCCUPIED GAP STATES

The energy-dependent imaginary part of the dielectric function, $\varepsilon_2(h\nu)$, is directly determined by $\alpha(h\nu)$ as well as the energy-dependent refractive index, $n(h\nu)$, as shown below:[32,36]

$$\varepsilon_2(h\nu) = \alpha(h\nu)n(h\nu)hc/2\pi h\nu, \tag{1}$$

where $E = h\nu$, represents the energy of the photon, $n(h\nu)$ is the energy-dependent refractive index, h is the Planck constant and c is the speed of light in vacuum. It was shown by Jackson *et al.*[32] that $\varepsilon_2(h\nu)$ for hydrogenated amorphous silicon is expressed as

$$\varepsilon_2(h\nu) = 4.3 \times 10^{-45} J_{DOS}(h\nu)R^2(h\nu), \tag{2}$$

and Eqs. (1) and (2) result in $J_{DOS}(h\nu)$ as

$$J_{DOS}(h\nu) = (\alpha(h\nu)n(h\nu)hc/2\pi h\nu)/(4.3 \times 10^{-45}R^2(h\nu)). \tag{3}$$

In these equations, $R^2(h\nu)$ stands for the average dipole matrix element squared and $J_{DOS}(h\nu)$ is the joint density of states function. The unit of $J_{DOS}(h\nu)$ is $cm^{-6}\,eV^{-1}$ and that of $R^2(h\nu)$ is $Å^2$. It was shown that $R^2(h\nu)$ is almost constant up to 3.5 eV and has a value of 10 $Å^2$.[32] For the higher energy region, well above the bandgap energy, $J_{DOS}(h\nu)$ defining the optical transitions from the electron-occupied parabolic valence band states into the empty parabolic conduction band states was defined by $J_{EE}(h\nu)$ as[33–35]

$$J_{EE}(h\nu) = \left(\frac{\pi}{8}\right)N_{co}N_{vo}(h\nu\text{-}E_{CD})^2, \tag{4}$$

where N_{co} and N_{vo} are the prefactors of the density of states function for conduction and valence bands, respectively, with the unit of $cm^{-3}\,eV^{-3/2}$ and E_{CD} defines the Cody gap of the sample. By using Eqs. (2) and (4), one can obtain that $\varepsilon_2(h\nu)$ can be re-expressed as

$$\varepsilon_2(h\nu) = 1.7 \times 10^{-44}(h\nu - E_{CD})^2. \tag{5}$$

When Eq. (5), known as the Cody equation,[39] is plotted as $[\varepsilon_2(h\nu)]^{1/2}$ vs photon energy, $h\nu$, the intercept at the energy axis gives the Cody gap, E_{CD}, of the sample and the slope provides the product $(N_{co}\,N_{vo})^{1/2}$, from which the theoretical $J_{EE}(h\nu)$ is calculated independently for the sample investigated. For undoped a-Si:H films, it is not possible to routinely obtain the experimental $\varepsilon_2(h\nu)$ spectrum of each sample down to the sub-bandgap energies due to experimental limitations of the techniques. However, the refractive index of undoped a-Si:H, $n(h\nu)$, was shown to be not a strongly varying function among different undoped a-Si:H samples

and presents a standard variation as a function of energy, as experimentally presented by Klazes *et al.*[37] A tenth-order polynomial fit function to this experimental refractive index data was generated and used for the analysis of the optical data of undoped a-Si:H films for the energy region from 0.7 to 3.4 eV.[36] In this paper, we have used that tenth-order polynomial fit function of n(hν), as kindly provided by Professor S. K. O'Leary, to calculate the $\varepsilon_2(h\nu)$ spectrum of each sample studied by using the α(hν) spectrum of the lowest dc bias light DBP measurement in order to derive the numerical values of E_{CD} and (N_{co} N_{vo}) as well as $J_{DOS}(h\nu)$.

In addition, the energy-dependent density of electron-occupied gap states, $kN_{gap}(h\nu)$, was obtained by taking the derivative of the α(hν) spectrum as defined previously,[40]

$$kN_{gap}(h\nu) = (h\nu)\left[\frac{d\alpha}{dE}\right] - \alpha(h\nu), \tag{6}$$

where k is a constant related to optical transitions.[32] Since the numerical value of the constant k cannot be obtained experimentally for each a-Si:H film, $kN_{gap}(h\nu)$ presents a relative spectrum, which can finally be normalized to an absolute number N_{VT} at energy E_{VT} as $N_{VT}(E_{VT}) = N_{vo}(E_{VT} - E_V)^{1/2}$, using N_{vo}, a prefactor of the density of states function obtained from the slope of the Cody plot of the sample. $(E_{VT} - E_V)$ was taken to be 25 meV as generally practised in the literature[36] and $E_{CD} = E_C - E_V$, which defines the Cody gap of the sample[39] obtained from the Cody plot. The density of the exponential occupied valence band tail states, $N_{VB}(E) = N_{VT}\exp[-(E_{VT} - E)/E_{ov}]$, was calculated by using the slope E_{ov} of the α(hν) spectrum, E_{VT}, and the prefactor N_{vo} of the sample, and then subtracted from the absolute $kN_{gap}(h\nu)$ spectrum to get the net energy-dependent density of electron-occupied midgap states located below the dark Fermi level. Finally, Gaussian defect distributions $[N(E) = (N_T/\sigma(2\pi)^{0.5})\exp(-(E-E_x)^2/(2\sigma^2))]$ with well-defined energy at a peak position, E_x, total density, N_T, and a half-width, $W = 2.355\sigma$, were defined to obtain the best fit to the resulting net energy-dependent density of electron-occupied midgap states.

IV. NATIVE DEFECT STATES IN THE ANNEALED STATE

The sub-bandgap absorption spectra, α(hν), of hydrogenated amorphous silicon films obtained from the photoconductivity methods are very sensitive to the density, distribution, energy positions, and the occupation of these defects, which can easily be modified by changing the light intensity. In order to have reliable and accurate photoconductivity measurements, the co-planar contacts of the sample studied must have and maintain the Ohmic nature for all voltages used for the measurements and after all experimental conditions that the sample has been exposed to. In Fig. 1, photoconductivity vs applied voltage measured from the embedded co-planar contacts of the sample is shown for four different conditions of the sample used in this work. Embedded contacts of the sample shown in the inset of Fig. 1 maintained their Ohmic nature for all measurements carried out in this study.

The raw DBP yield spectra of the annealed state, Y_{DBP}, measured under three different dc bias light intensities and the corresponding optical transmission spectrum of the sample are

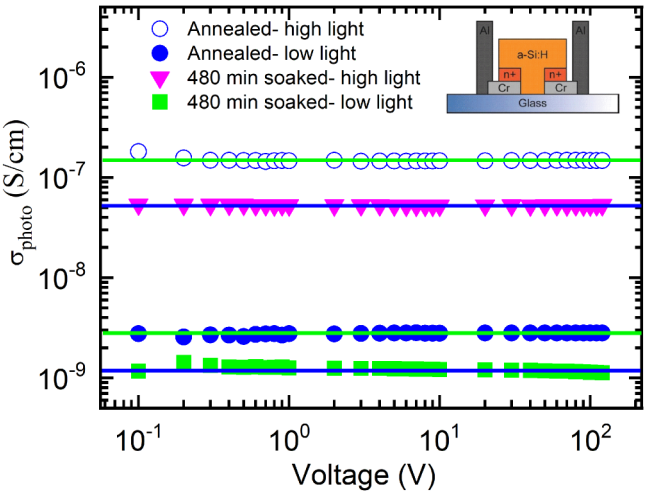

FIG. 1. Photoconductivity vs applied dc voltage measured from the Ohmic embedded contacts of the sample. In the inset, contact geometry of embedded contacts of sample is shown.

presented in Figs. 2(a) and 2(b), respectively. The phase of the DBP signal and the dc/ac ratio of ac photocurrents for each dc bias light measurement are also shown in the inset of Figs. 2(a) and 2(b), respectively. In order to have the ac photoconductivity spectrum, Y_{DBP}, directly proportional to the absorption coefficient spectrum, α(hν), at all energies, a sufficiently high intensity of dc bias light must be used to achieve a dc/ac ratio of photocurrents much higher than unity. This can only be satisfied for the high dc bias light spectrum for all energies as shown in the inset of Fig. 2(b). However, at a high dc bias light condition, artificially increased occupation of the midgap states above the Fermi level is probed by the DBP spectrum, which results in higher defect absorption in sub-bandgap energies. In order to probe the distribution of the true density of electron-occupied gap states present in the dark, the dc bias light intensity of DBP must be decreased as much as possible. For lower dc bias light intensities, an accurate DBP signal with a dc/ac ratio much higher than unity can only be measured below the exponential valence band tail. For this reason, the Y_{DBP} spectrum labeled as dc bias light-low2 in Fig. 2 (a) is first normalized at 1.52 eV to the spectrum of the high dc bias light [as shown by a red arrow in the inset of Fig. 2(b)]. Finally, the Y_{DBP} spectrum of the dc bias light-low1 is normalized at 1.40 eV to that of the dc bias light-low2, at which the dc/ac ratio is around $30 \gg 1$, as seen in the inset of Fig. 2(b). At the lowest intensity of dc bias light (called dc bias light-low1), the flux of dc bias light equals $6-8 \times 10^{12}\ cm^{-2}\ s^{-1}$, which approximately corresponds to 10^{-5} of AM1.5 light intensity. Under this condition, the distribution of electron-occupied midgap states probed by the DBP is closer to that below the dark Fermi level and results in a spectrum equivalent to that of CPM.[30] This is confirmed by the phase of the DBP signal of the dc bias light-low1 spectrum that is presented in the inset of Fig. 2(a), showing no significant change from the valence band tail edge down to 0.7 eV, as generally observed in the phase of

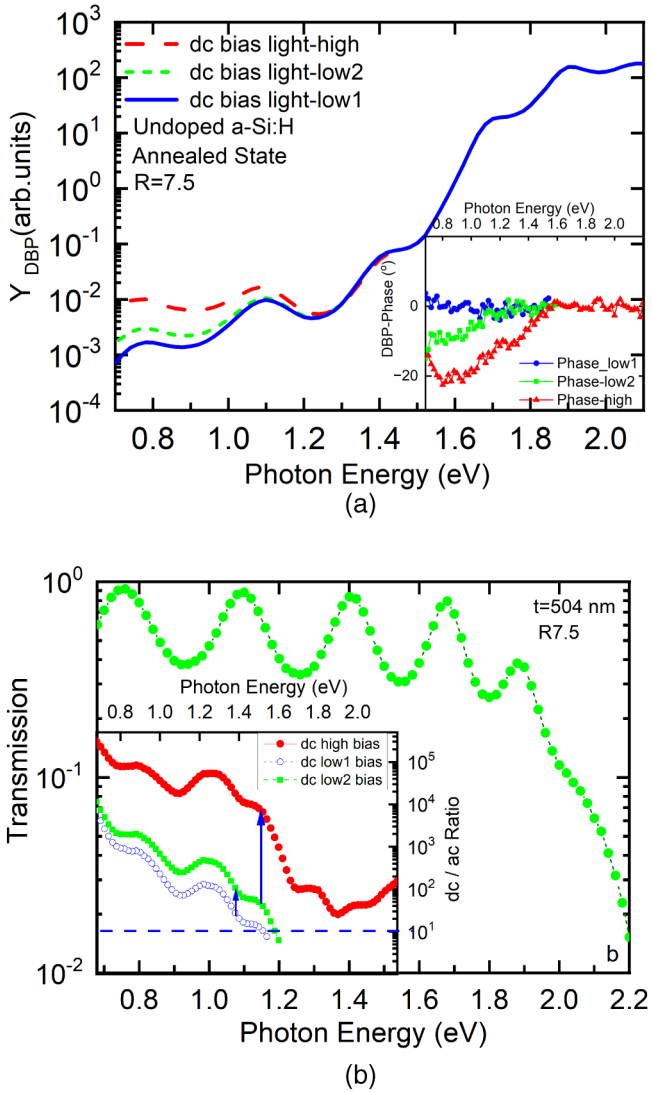

FIG. 2. (a) Relative DBP yield spectra of undoped a-Si:H in the annealed state measured with three different dc bias light intensities. In the inset, the phase of DBP signals is shown for corresponding dc bias light measurements. (b) Optical transmission spectrum in absolute scale simultaneously measured from the back of the sample. In the inset, dc/ac ratios of photocurrents are presented for each DBP measurement.

the CPM signal.[41] When the intensity of the dc bias light increases, new unoccupied gap states located above the Fermi level become partially occupied by electrons and are, thus, converted to recombination centers, which cause a change in the phase of the DBP signal as seen in the inset of Fig. 2(a), while they also result in an increase in the Y_{DBP} spectrum at lower energies. Although the intensity dependence of DBP spectra contains detailed information about the density, distribution, energy locations, and the nature of the gap states, in this study, we will focus only on the analysis of

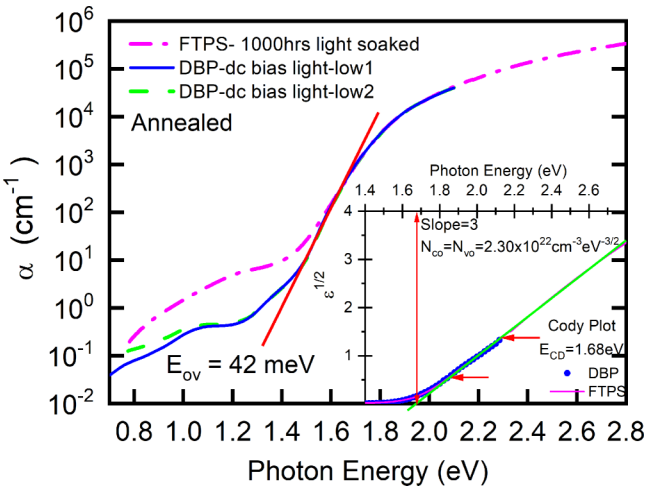

FIG. 3. Calculated absorption coefficient spectra of undoped a-Si:H in the annealed state are shown for two different DBP spectra and that measured by FTPS in the light soaked state. In the inset, the Cody plot is presented for both DBP and FTPS measurements.

the DBP spectrum measured with the lowest dc bias light (shown as dc bias light-low1) and calculate the corresponding absorption coefficient spectrum, α(hν), from which the energy dependence of the electron-occupied midgap defect states will be derived as presented below.

Fringe-free absolute α(hν) spectra in the annealed state for dc bias light-low1 and dc bias light-low2 are calculated from the corresponding Y_{DBP} and optical transmission spectra of the sample presented in Fig. 2 by using Ritter–Weiser optical equations.[38] It is seen that the calculated α(hν) spectra involve no interference fringes, which are naturally removed by optical equations and the fact that the transmittance is measured in exactly the same spot as where the DBP measurement is conducted, meaning that the interference fringes present in the transmittance and photocurrent spectra have extrema at exactly same energy positions. Furthermore, no normalization procedure of Y_{DBP} has been carried out here, in contrast to the general approach used in the conventional DBP method.[18,31,42] The α(hν) spectra shown in Fig. 3 indicate that increasing the dc bias light intensity causes an increase in α(hν) below 1.2 eV without affecting the occupation of defects at higher energies. The characteristic slope of the valence band tail absorption was found to be 42 meV, indicating a high quality of amorphous silicon studied in this work. The accuracy of the calculated α(hν) spectrum is also compared with that independently measured by the FTPS method for this a-Si:H film and is presented in Fig. 3. The FTPS spectrum of the sample was measured after 1000 h of AM1.5 light soaking at Delft University of Technology and under a higher intensity of white light (~0.01 suns) such that a significant increase in the α(hν) in the sub-bandgap region existed from that of the annealed DBP spectrum. However, there is a good overlap between the two spectra above the exponential absorption region, indicating that the improved DBP method allows us to obtain the absolute α(hν) spectrum of the samples independently

and accurately, in contrast to the conventional DBP method,[18,31,42] requiring fringe removing procedures and normalization at energy around the bandgap energy to an absolute α(hν) measured by another technique to get a fringe-free absolute α(hν) spectrum.

The α(hν) spectrum obtained in Fig. 3 is proportional to the imaginary part of the dielectric constant, $\varepsilon_2(h\nu)$, as well as to the refractive index, n(hν), as presented in Eq. (1). As first approximation, we have used the tenth-order polynomial fit function of n(hν) created for the original Klazes data[37] by Thevaril and O'Leary[36] and calculated the $\varepsilon_2(h\nu)$ spectrum of the sample by using the α(hν) spectra of dc bias light-low1 as well as that of FTPS (data not shown). In the inset of Fig. 3, the Cody plot of the sample obtained from Eq. (5) is presented for both DBP and FTPS spectra. It is clearly seen that a perfect straight line is obtained for the energy region above 1.9 eV as generally presented,[39] where only optical transitions from the electron-occupied parabolic valence band extended states to the empty parabolic conduction band extended states define the α(hν) spectrum. The two spectra overlap very well and the DBP spectrum alone provides a sufficient energy region above the bandgap to obtain the Cody gap of the sample from the intercept at the energy axis. It was found that the Cody gap of the sample, E_{CD}, is 1.68 eV and the slope of the straight line provides the value of $(N_{co}N_{vo})^{1/2}$, which equals $2.3 \times 10^{22}\ cm^{-3}\ eV^{-3/2}$, thus underlining the accuracy of both photocurrent measurement methods.

Finally, the values of E_{CD} and $(N_{co}N_{vo})$ were used to calculate the joint density of states function, $J_{EE}(h\nu)$, of the sample using Eq. (4) and presented in Fig. 4. $J_{EE}(h\nu)$ is the joint density of states function due only to optical transitions from electron-occupied parabolic valence band extended states into empty parabolic conduction band extended states, dominating the spectrum only above the Cody gap, E_{CD}. However, the α(hν) spectrum measured by either DBP or FTPS is determined by all optical transitions from the electron-occupied defect states into the empty conduction band extended states. For this reason, we have calculated the joint density of states functions of the experimental DBP and FTPS spectra, $J_{DBP}(h\nu)$ and $J_{FTPS}(h\nu)$, by using the corresponding the α(hν) spectrum of each measurement as well as the energy-dependent refractive index spectrum, n(hν), provided in the literature.[36,37] These are presented in Fig. 4 together with the calculated $J_{EE}(h\nu)$ of the sample. It is seen that the shape and magnitude of the spectra, $J_{DBP}(h\nu)$, $J_{FTPS}(h\nu)$, and $J_{EE}(h\nu)$, overlap perfectly above 1.9 eV, indicating that both photoconductivity methods of the improved DBP and the FTPS probe the same optical transitions from electron-occupied parabolic valence band extended states to unoccupied parabolic conduction band extended states at an energy region above 1.90 eV. However, for the energies below E_{CD}, other optical transitions from electron-occupied localized defect states into empty conduction band extended states will contribute to the α(hν) spectrum as measured by DBP and FTPS methods. As can be seen from Fig. 4, optical transitions from electron-occupied exponential valence band tail states dominate the spectrum down to 1.5 eV in the $J_{DBP}(h\nu)$ spectrum, where the slope of the straight line represents the characteristic slope E_{ov} of valence band tail states, which is the same as that obtained from the α(hν) spectrum shown in Fig. 3. Since $J_{DBP}(h\nu)$ of the dc bias light-low1 below 1.5 eV is only due to optical transitions from the electron-occupied midgap states located below the dark Fermi level into the unoccupied conduction band extended states, detailed information about the electron-occupied midgap states can be obtained from $J_{DBP}(h\nu)$ or the α(hν) spectrum. This was first reported by Pearce *et al.*[40] who noted that the energy-dependent electron-occupied gap states, $kN_{gap}(h\nu)$, can be derived from the deconvolution of the absolute α(hν) spectrum and are used to identify the midgap defect states.

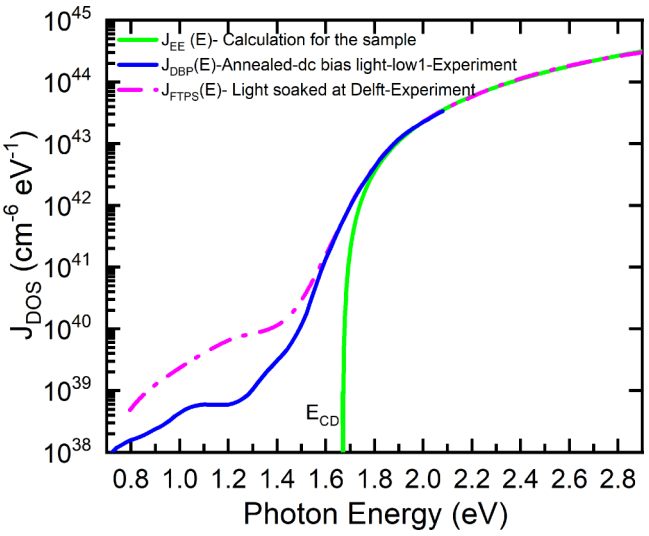

FIG. 4. The joint density of states functions of the sample, $J_{FTPS}(h\nu)$ and $J_{DBP}(h\nu)$, calculated by using the absorption coefficient spectra presented in the Fig. 3 of FTPS and DBP measurements, respectively. In addition, the joint density of states function, $J_{EE}(h\nu)$, shown in this figure defines only optical transitions from the electron-occupied parabolic valence band extended states to the empty parabolic conduction band extended states, calculated for the sample by using the numerical values of E_{CD} and $N_{co}N_{vo}$ obtained from the Cody plot presented in the inset of Fig. 4 according to Eq. (3).

In this study, the energy dependence of electron-occupied gap states, the native defects of the annealed state, the $kN_{gap}(h\nu)$ spectrum, was calculated from the derivative of the α(hν) spectrum using Eq. (6) as defined in Sec. III. In Fig. 5, the energy dependence of the total electron-occupied gap states is shown together with the occupied valence band tail states of the sample calculated using the parameters E_{ov}, N_{vo}, N_{VT}, and E_{CD} of the sample as obtained above. It is seen that the electron-occupied midgap states dominate the spectrum below 1.42 eV, above which the occupied valence band tails increase exponentially until the band edge. Finally, the net energy-dependent density of electron-occupied midgap states is obtained by subtracting the occupied valence band tails from the total $kN_{gap}(h\nu)$ spectrum and presented in Fig. 6. The resulting spectrum was separated into several Gaussian types of defect states with their characteristic peak energy positions, total density, and half-widths to obtain the best fit for the data. It was found that four different Gaussian-type defect distributions can be identified and named as A, B, C, and X states following the previous nomenclature.[13–15,28,29]

The peak energy positions of these defect states are found at photon energies of 0.89 ± 0.05, 1.0 ± 0.01, 1.34 ± 0.01, and

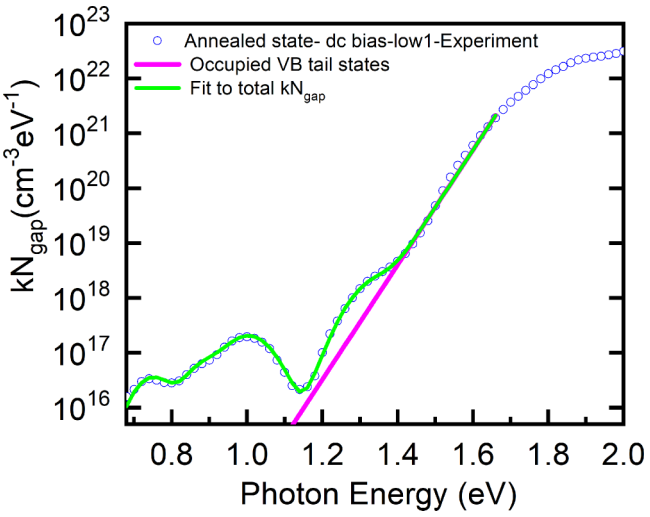

FIG. 5. Energy dependence of total electron-occupied gap states, kN_{gap}, obtained for the DBP spectrum of dc bias light-low1 and calculated occupied valence band tail states for undoped a-Si:H in the annealed state.

0.75 ± 0.01 eV for A, B, C, and X states, respectively. The best fit to the net experimental $kN_{gap}(h\nu)$ spectrum was obtained for the total density of $(6.0 \pm 0.2) \times 10^{15}$, $(2.8 \pm 0.1) \times 10^{16}$, $(2.0 \pm 0.1) \times 10^{17}$, and $(4.0 \pm 0.1) \times 10^{15}$ cm^{-3} for A, B, C, and X states, respectively. Their half-widths were similar and vary within 120 ± 15 meV as shown in Fig. 6. As a summary, four different native defect states located below the dark Fermi level were identified by using the improved DBP method, among those, C states closer to the valence band tail have the highest density and X states in the middle of bandgap have the lowest density.

V. STAEBLER–WRONSKI DEFECTS IN THE LIGHT-SOAKED STATE

The Staebler–Wronski effect[1] appears to be an intrinsic property of undoped a-Si:H that is typically used to explain degradation in the photoconductivity of the sample under extended illumination. In order to see a significant effect of light soaking, an undoped a-Si:H sample investigated in this work was illuminated by AM1.5 equivalent white light for 480 min as the sample was mounted in a high vacuum cryostat. The temperature of the sample was set to 20 °C and kept constant during light soaking by the temperature controller of the liquid nitrogen-cooled cryostat. The time dependence of the photoconductivity during light soaking is recorded every 5 min by a computer program and presented in the inset of Fig. 7. It is clearly seen that σ_{photo} (AM1.5) degrades with a power law of $t^{-\beta}$, where the exponent was calculated to be $\beta = 0.20 \pm 0.02$, which is different from the commonly reported $t^{-1/3}$ power law,[4,6,7] but in line with the earlier reported data.[18] σ_{photo} as a function of the intensity of red light was also measured within 5 min right after terminating light soaking in order to prevent the effects of room temperature annealing[20–23,25] of the light-induced defects on the measured photoconductivity. In Fig. 7, the results of $\sigma_{photo,}$ in both annealed and light-soaked states, were presented as a function of the photon flux to quantify the amount of degradation. σ_{photo} decreased by a factor of six from annealed values. The exponent γ of the σ_{photo} on the light flux was calculated to be 0.85 in annealed and light-soaked states.

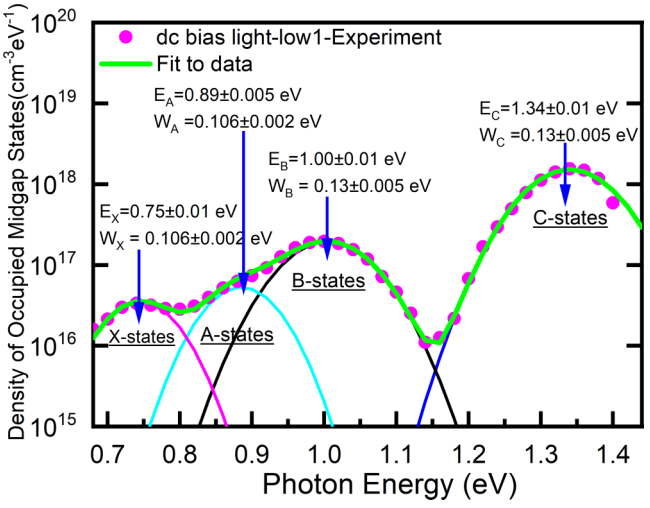

FIG. 6. Energy dependence of electron-occupied midgap states, native defect states (green solid line), in the annealed state of undoped a-Si:H obtained from the deconvolution of the $\alpha(h\nu)$ spectrum corresponding to the dc bias-low1 experiment. Four different Gaussian type midgap defect states labeled as A, B, C, and X states are identified at well-defined peak positions and half-widths.

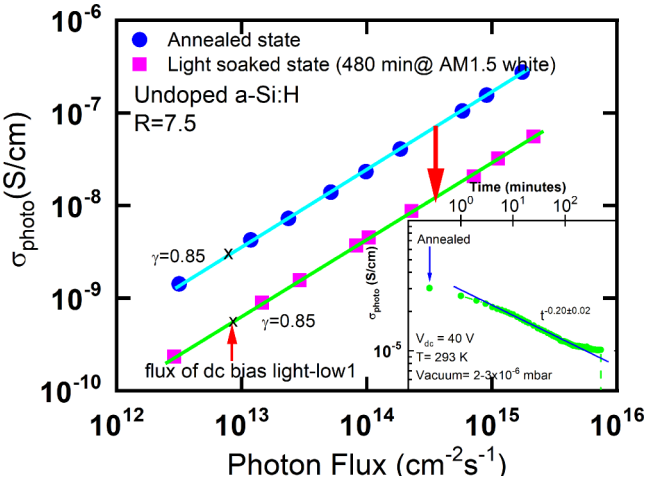

FIG. 7. Steady-state photoconductivity of undoped a-Si :H in the annealed state and after 480 min of light soaking carried out in vacuum under AM1.5 white light. In the inset, time-dependent σ_{photo} recorded during degradation under AM1.5 white light is shown. The flux of dc bias light-low1 of DBP measurement is also indicated.

The degradation of σ_{photo} was attributed to the creation of light-induced defect states due to the Staebler–Wronski effect.[1] These defects are located in the bandgap of a-Si:H and detected directly by electron paramagnetic resonance (EPR)[2,3] as well as by sub-bandgap absorption methods.[18] EPR detects only the paramagnetic defects called the D^o states. However, the sub-bandgap absorption spectrum measured by photoconductivity methods such as CPM[30] and DBP[18,31,42] probes both D^o and non-D^o defect states. We have applied the improved DBP method in the light-soaked state and measured Y_{DBP} spectra for different dc bias light intensities right after light soaking (which was within 30 min after soaking ended). In Fig. 8, the Y_{DBP} spectra are shown for three different dc bias light intensities. It is seen that a similar Y_{DBP} spectrum of the annealed state as well as the phase of the DBP signal given in the inset are obtained after light soaking. The phase of dc bias light-low1 measurement is constant at all energies indicating that the distribution of electron-occupied defect states below the dark Fermi level was not significantly altered by the low intensity of the bias light used in DBP. The α(hν) spectrum in the light-soaked state corresponding to dc bias light-low1 was calculated using the Y_{DBP} (low1) and optical transmission spectra and presented in Fig. 9 together with that of the annealed state. In the inset, relative Y_{DBP} spectra measured under dc bias light-low1 are also shown in both annealed and light-soaked states to see the relative change of the raw DBP spectrum in the sub-bandgap region. There exists a significant increase in α(hν) values below the valence band tail due to an increased density of the electron-occupied midgap defects created by light soaking. It is clearly seen that there exists an asymmetric increase in α(hν) in the sub-bandgap region.

The energy dependence of the electron-occupied defect states in the light-soaked state, now called the Staebler–Wronski defects, was calculated by taking the derivative of the light-soaked α(hν) spectrum. In Fig. 10, the absolute total $kN_{gap}(h\nu)$ spectrum is shown together with the calculated occupied exponential valence band tail states. Similarly carried out in the annealed state, the exponential valence band tail distribution is subtracted from the total $kN_{gap}(h\nu)$ spectrum and the resulting spectrum is fit to four

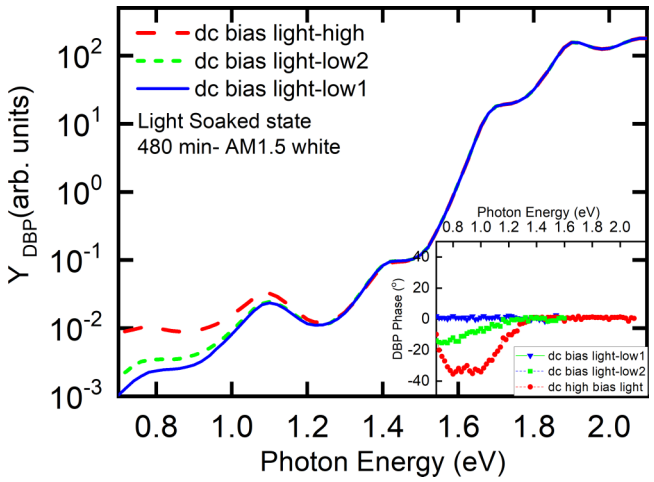

FIG. 8. Relative DBP yield spectra of undoped a-Si:H in the light-soaked state for three different dc bias light intensities. In the inset, the phase of DBP signals is shown for the corresponding dc bias light measurements.

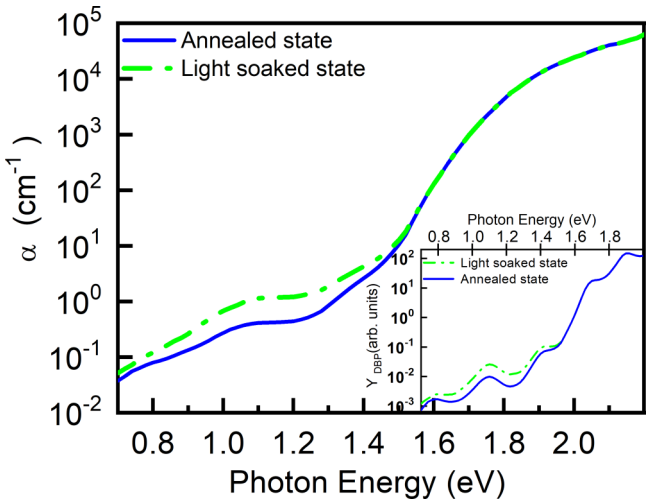

FIG. 9. Absorption coefficient spectra of undoped a-Si:H in the annealed and light-soaked states calculated from the dc bias light-low1 spectra and the optical transmission spectrum. In the inset, corresponding raw Y_{DBP} spectra of the sample in the annealed and light-soaked states are presented for dc bias light-low1.

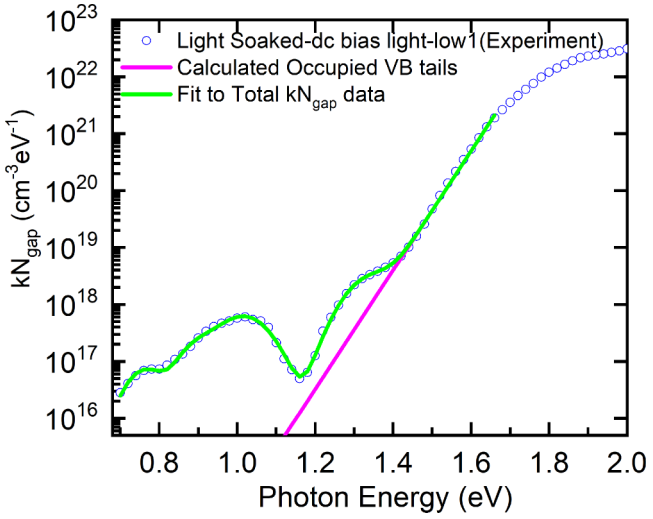

FIG. 10. Energy dependence of total electron-occupied gap states in the light-soaked state obtained for the DBP spectrum of dc bias light-low1 and calculated occupied valence band tail states. The best fit is obtained by using exponential valence band tail states and four different Gaussian defect states with the same peak positions and half-widths of native defect states.

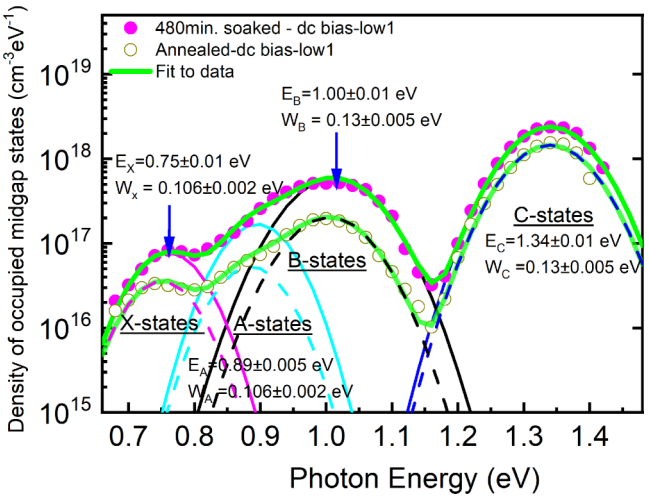

FIG. 11. Energy dependence of electron-occupied midgap states, Staebler–Wronski defects, in the light-soaked state obtained from the deconvolution of $\alpha(h\nu)$ spectrum corresponding to the dc bias-low1. Four different Gaussian type midgap defect states at the same energy positions of A, B, C, and X states of the annealed state are identified. The density of A, B, C, and X states increases unevenly after 480 min light soaking. The numerical values of the densities of the Gaussians are given in the text.

different Gaussian-type defect states at peak positions and total densities as shown in Fig. 11. These Gaussian-type defect states obtained in the light-soaked state are found to be almost at same energy positions and same half-widths of the native defects found in the annealed state, while their density increased by light soaking. The total density of A, B, C, and X states increased to $(1.90 \pm 0.05) \times 10^{16}$, $(8.60 \pm 0.1) \times 10^{16}$, $(3.3 \pm 0.1) \times 10^{17}$, and $(8.80 \pm 0.06) \times 10^{15}$ cm^{-3}, respectively. The increase in their density is by a factor of 3.2, 3.0, 1.65, and 2.2 for A, B, C, and X states, respectively, indicating that each defect distribution increased at a different rate. The intensity-dependent σ_{photo} shown in Fig. 7 decreased approximately by a factor of six at all flux levels showing that degradation in σ_{photo} cannot be correlated directly to the density of either of these defects alone. Their capture cross sections are also required to be considered in the degradation of σ_{photo} as well as in the occupation of these defects causing the intensity dependence of the sub-gap absorption coefficient spectrum as measured by DBP.

In this study, the presence of multiple defect states and their absolute densities and energy positions were studied in the annealed as well as in the light-soaked states. In every experimental work, parameters measured and new parameters derived from the measured ones will involve a certain degree of error that includes experimental error due to equipment, sample handling, and ambient conditions, as well as propagation of errors in the derivation of new parameters from experimental results. First of all, possible experimental errors can be introduced in the simultaneous measurement of raw DBP and optical transmission spectra by lock-in amplifiers. The phase of a lock-in amplifier is very sensitive to experimental error if the signal-to-noise ratio is low. In this context, the phase of the DBP signal shown in the inset of Figs. 2(a) and 8 is a good indication that raw DBP and T spectra are measured accurately within a small experimental error. The variation in the phase of the DBP low-1 spectrum is within a few degrees around the set angle of zero degrees between adjacent points. The calculated absorption coefficient spectrum is smooth and contains no remaining interference fringes, indicating that light is uniformly absorbed in the film and peak positions of fringes are exactly at same energy locations for both DBP and T spectra. In addition, the calculated absorption coefficient spectrum of DBP overlaps perfectly above the valence band tails with that of the independently measured absorption coefficient spectrum by FTPS for the same sample. Therefore, uncertainty in the absolute absorption coefficient spectrum is within an experimental error limit that is not greater than a few percent. This is also supported by the J_{DOS} figures of DBP and FTPS as compared with the theoretical J_{EE} of the sample. As a result, it is not suitable to present any error bars in such figures up to Fig. 5, which will be smaller than the symbol size. Hereby, we note that such limited error values are significantly smaller than typical variations in the density of the different sub-bandgap distributions, which can easily vary over the orders of magnitude instead of a few percent or tens of percent.

The energy positions and absolute densities of Gaussian-type defects located in the sub-bandgap energy region were obtained from the energy-dependent electron-occupied defect distribution, kN_{gap} (E), given by Eq. (6), where uncertainties in the parameters might cause the propagation of error in kN_{gap}; here Δ(E) is the uncertainty in energy E defined by the resolution of the monochromator, $\Delta[d(\alpha)/dE]$ is the uncertainty in the derivative of α, and $\Delta(\alpha)$ is the uncertainty in the absolute absorption coefficient, α. By using a standard error propagation analysis, the uncertainty in kN_{gap}, $\Delta(kN_{gap})$ is calculated for the whole spectrum. It is derived that the error of kN_{gap} is less than 5%, as shown in Fig. SI 2 in the supplementary material. kN_{gap} in the subgap region is determined by the sum of the electron-occupied X, A, B, and C states. Therefore, the uncertainty in each Gaussian-type defect density must be lower than that of kN_{gap}. The density of each Gaussian defect was an independent parameter and adjusted to get the best fit to the net kN_{gap} spectrum in the subgap region. Another possible error in quantifying the absolute density of Gaussian defects depends on the normalization of kN_{gap} at energy E_{VT} to N_{VT} as defined in Sec. III. The numerical value of N_{VT} is defined by N_{vo} of the sample, which was obtained from the slope of the Cody plot as presented in the inset of Fig. 3. Both FTPS and DBP results give a perfect fit to a linear slope of the Cody plot in a wider energy region such that the inaccuracy in N_{vo} is negligible. Finally, normalized kN_{gap} to N_{VT} at energy E_{VT} will allow us to determine the absolute numerical values of each Gaussian defect contributing to total kN_{gap}, which will be the summation of A, B, C, and X as well as the exponential valence band tail states below energy E_{VT}. Then additional errors in the density and energy positions of Gaussians are defined according to the best fits to the kN_{gap} spectrum, which is indicated in Figs. 6 and 11, and the limits are stated explicitly in the text. The error bars indicated in the other graphs in determining the slope of variables stay within the experimental error limit.

In order to confirm the validity and reproducibility of multiple defects detected in the bandgap of undoped a-Si:H, we have extended our investigations to other sister samples deposited under identical preparation conditions of R = 7.5. We have measured several sister samples in the annealed as well as in the light-soaked states and followed the same method of analysis described above. The results of one of the sister samples having the same embedded contact geometry are shown in Figs. SI1(a)–1(c) in the supplementary material for both annealed and light-soaked states. Similar to that found above, four different Gaussian-type defect distributions labeled as A, B, C, and X were also identified for best fits to the density of electron-occupied midgap states. Their peak energy positions and half-widths are around the same values of defects as found in Fig. 6. Mainly, the total density of Gaussian distributions increased by light soaking, while slight differences in densities between samples are ascribed to a sample-to-sample variation.

As a result, we can conclude from these results that the native and Staebler–Wronski defects are the same types of defects located almost at the same peak energy positions; only their density increases at different rates by extended light soaking. Therefore, the time-dependent creation of each Gaussian defect state will be important and provides essential information in understanding the degradation of solar cell devices under AM1.5 light as well as the changes in the steady state photoconductivity of films measured at different generation rates.

VI. KINETICS OF STAEBLER–WRONSKI DEFECTS

Even though extensive research has been carried out in the literature for the kinetics of the SWE,[6,7,18,19,22,24] there is no consistency among the research results. The kinetics of light-induced defect creation in films and solar cells was reported to depend on the nanostructure of the sample, sample history, and sample temperature as well as on the intensity of light.[15,18,19,22,23] Therefore, in order to investigate the kinetics of light-induced defect creation in undoped a-Si:H films, certain standard test conditions for experimentation before and after the light soaking procedure need to be established for reliable comparisons of results carried out in different laboratories as well as among the samples studied in the same laboratory. First of all, the sample temperature during light soaking, the intensity of white light, ambient of the sample, and the defect density in the annealed state must be identical and reproducible. In this study, the sample temperature was fixed to 20 °C during light soaking by using a temperature controller in a liquid nitrogen-cooled high vacuum cryostat. The intensity of white light was adjusted to AM1.5 intensity using a calibrated photodiode and the DBP spectrum for dc bias light-low1 was measured to obtain the total density of native A, B, C, and X states from the analysis of the α(hν) spectrum after each annealing procedure carried out before each light soaking step. In order to provide the reproducibility of the annealed state, dark conductivity vs inverse temperature was recorded after each annealing procedure as the sample cools to room temperature, and those results are presented in Fig. 12. It is seen that reproducible and the same reversible annealed state was obtained after annealing of each light soaking step within the experimental error.

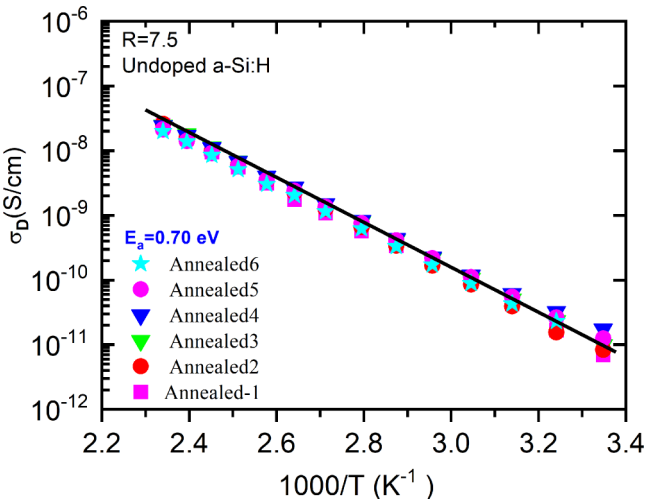

FIG. 12. Arrhenius plot of dark conductivity vs inverse temperature for the undoped a-Si:H sample measured after annealing of each light-soaked state as sample cools to room temperature.

After complete measurement processes of photoconductivity and DBP spectra of each annealed state, the analysis of the α(hν) spectrum was carried out to determine the density of Gaussian distributions present at each annealed state as described above. The total density of A, B, C, and X states obtained for each annealed state is shown in Fig. 13. It can be seen that a reproducible annealed state was provided for the initial density of Gaussian distributions before starting the degradation kinetics of the Staebler–Wronski effect. In the annealed state, it was found that the density

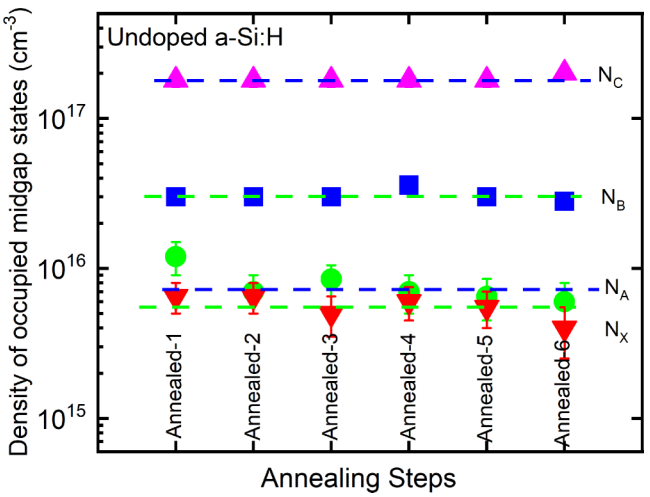

FIG. 13. The density of Gaussian defect states obtained after each annealing procedure carried out after each light soaking step of the undoped a-Si:H sample used in this study. Lines are guide to eye.

of native C states closer to the valence band tails is the highest and equals $(2.0 \pm 0.2) \times 10^{17}$ cm^{-3}. The total density of native B, A, and X states is stabilized at constant values of $(3 \pm 0.4) \times 10^{16}$, $(7 \pm 0.5) \times 10^{153}$, and $(6 \pm 0.5) \times 10^{15}$ cm^{-3}, respectively, without having any significant change in peak energy positions and half-widths of Gaussian distributions. Uninterrupted single-step light soaking as defined before[18] at a constant temperature of 20 °C in high vacuum was applied from the annealed state until the end of the light soaking period. Real-time recording of σ_{photo} (AM1.5) during light soaking for the undoped a-Si:H film studied above is shown in Fig. 14 for light soaking periods of 6, 20, 60, 200, and 480 min. It is seen that light soaking started from almost the same reproducible annealed σ_{photo} value of $3.2 \pm 0.2 \times 10^{-5}$ S/cm, which was recorded as the light is on at t = 0 s and followed the same time-dependent degradation as all the curves overlap. Two different regions can be clearly identified in the degradation of AM1.5 photoconductivity. In region I, a straight line can be fit to the log–log plot of σ_{photo} vs time, and it extends from the beginning to the end of approximately 2 h of light soaking where all the light soaking curves overlap. σ_{photo} obeys the $t^{-\beta}$ power law. The exponent β was calculated to be 1/5 (0.20 ± 0.02). In region II, beyond 2 h of soaking, a tendency toward saturation or to a lower time dependence of σ_{photo} was observed for this sample as well as for other sister samples investigated (data not shown). Once the light soaking has ended, the σ_{photo} vs flux for the light-soaked state under collimated He–Ne laser light was measured within 5 min right after soaking. The changes in σ_{photo} as a function of the soaking time recorded under low and medium flux values of red light are summarized in the inset of Fig. 14. The degradation of σ_{photo} measured at the high and low flux of red light can be fit to a single power law of $t^{-\beta}$ covering both regions, where β equals to 0.20 ± 0.02 for the medium flux of 1×10^{15} cm^{-2} s^{-1}, the same as that of σ_{photo} (AM1.5) degradation. However, σ_{photo} degrades at a slower rate with the exponent $\beta = 0.14 \pm 0.02$ for the measurement at a low flux of 1×10^{13} cm^{-2} s^{-1}. Even though there exists a tendency toward saturation in σ_{photo} (AM1.5) after 2 h, σ_{photo} at the lower and intermediate light intensities continue to degrade at the same rate. In order to understand the details of defect creation kinetics and their effects on σ_{photo} measured at low and medium light intensities as well as that on the α(hν) spectrum, the changes in the density of each Gaussian type defect identified in the bandgap of a-Si:H must be determined through the analysis of the α(hν) spectrum.

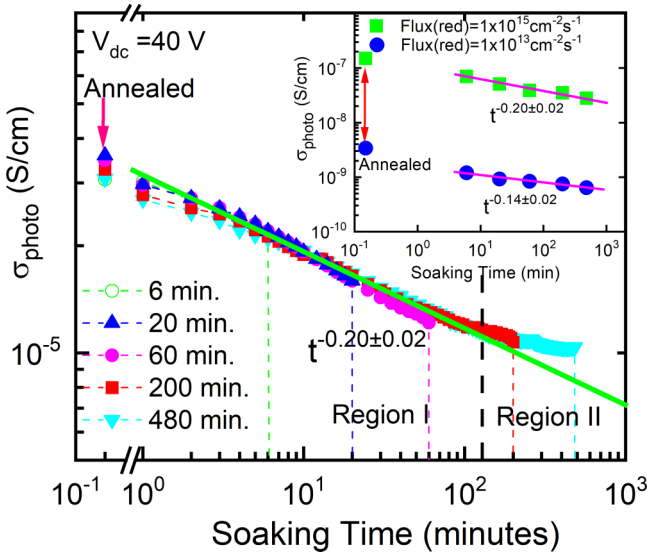

FIG. 14. Real time monitoring of photoconductivity changes measured during light soaking under AM1.5 white light. The dashed lines indicate the termination of the light soaking, for which photoconductivity drops to the level of dark conductivity. In the inset, photoconductivity vs time for the flux of 1×10^{13} and 1×10^{15} cm^{-2} s^{-1} of red light of He–Ne laser measured right after the end of each light soaking period.

The kinetics of light-induced defect creation studied by using sub-bandgap absorption methods have been extensively characterized by monitoring only the α(hν) values at a single energy, usually at E = 1.2 eV.[42,43] In this study, the kinetics of the light-induced defect creation have been investigated by monitoring both the changes in α(hν) at the peak energy values of each Gaussian defect as well as by monitoring the net increase in the density of these Gaussian distributions. For this reason, the $kN_{gap}(h\nu)$ spectrum, by taking the derivative of the α(hν) spectrum, measured right after each light soaking period for the dc bias light-low1 of the improved DBP method has been used to obtain the density, peak energy positions, as well as the half-widths of A, B, C, and X states. In Fig. 15(a), the α (hν) values recorded at peak energy positions of A, B, C, and X states are presented as a function of the light soaking time after subtracting the corresponding annealed α(hν) values shown in Fig. 13. Two different regions can be clearly identified in the changes of the α(hν) values recorded at peak energy positions of Gaussian defects. No significant time dependences of $\alpha_{net}(h\nu)$ $[=\alpha_{soaked}(h\nu) - \alpha_{annealed}(h\nu)]$ have been detected within the experimental error at peak energy positions of A and X states in both regions as seen in Fig. 15(a). Similarly, the $\alpha_{net}(h\nu)$ at the peak energy position of B and C states showed no significant time dependence in region I. However, the $\alpha_{net}(h\nu)$ of both B and C states exhibited a stronger time dependence in region II with a power low of t^{β}, where β equals 0.5 ± 0.02. In order to understand the contributions of individual Gaussian defect states to the measured α (hν) spectrum, the corresponding changes in the density of A, B, C, and X states were obtained from the best fits to $kN_{gap}(h\nu)$ spectrum calculated from the α(hν) spectrum of each light-soaked state. These changes are shown in Fig. 15(b) as a function of the light-soaking time, where the annealed state density of each Gaussian distribution was subtracted from light-soaked values. Two different time-dependent regions are identified for the light-induced changes in the density of A, B, and C states. In region I, the net increase in their density remained at constant values. In region II, the net change in the density of A state, N_A, increased very slowly and obeyed a power law of t^{β}, with the exponent $\beta = 0.10 \pm 0.02$. However, B and the C states presented a stronger dependence on the soaking time according to a power law of t^{β} where β equals 0.5 ± 0.02, representing the same power law of $\alpha_{net}(h\nu)$ shown in Fig. 15(a). The increase in the X state located in the middle of the bandgap was found to be independent of time.

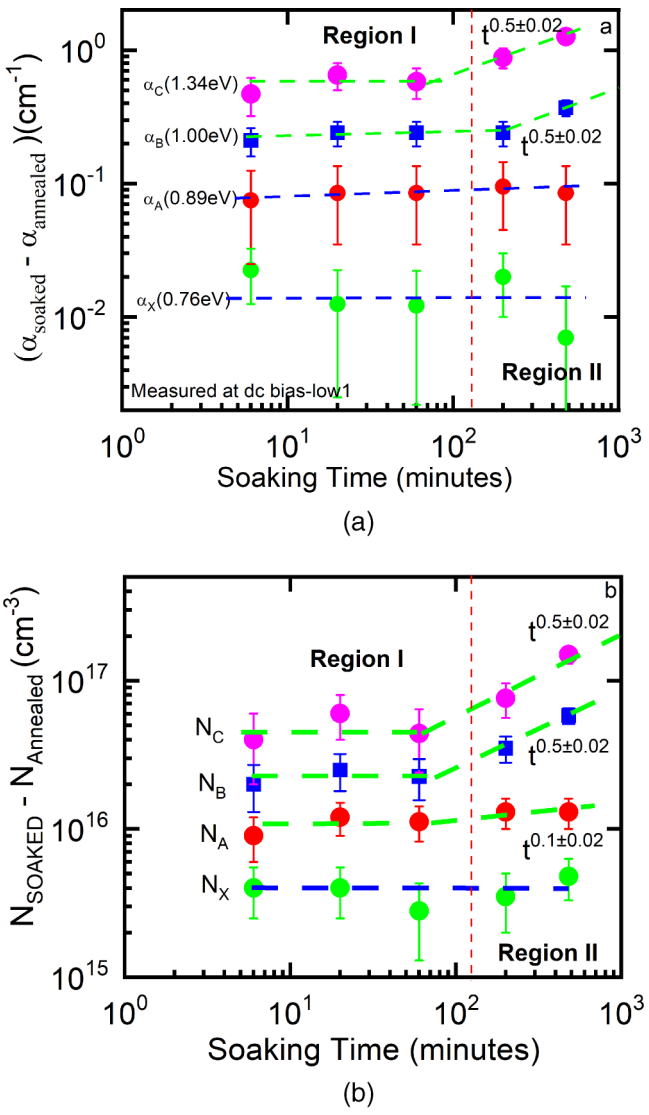

FIG. 15. (a) The changes in the values of α(hν) at the peak energy position of A, B, C, and X states vs time obtained from the measurement of dc bias light-low1, (b) the changes in the density of the Gaussian defect states of A, B, C, and X as a function of light soaking time obtained from the best fit to the spectrum of energy dependence of electron-occupied midgap states. Lines are guide to eye.

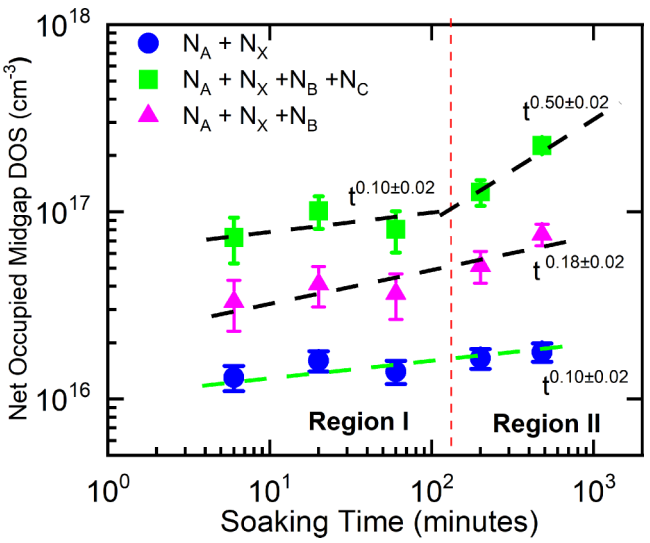

FIG. 16. The net changes in the total density of Gaussian distributions during light soaking obtained from the deconvolution of the α(hν) calculated from the dc bias-light low1 DBP measurement after each light soaking step. Annealed state values of each Gaussian are substracted from each corresponding soaked state value. Lines are guide to eye.

The net change in the density of the Gaussian defects correlates well with the time-dependent changes in $\alpha_{net}(h\nu)$ recorded at peak positions of Gaussian defects shown in Fig. 15(a).

There is no significant variation in the peak energy positions and half-widths of Gaussian distributions obtained for best fits to A B, C, and X states and stay within the values presented for annealed and light-soaked states data shown in Figs. 6 and 11, respectively. The peak energy positions and the half-widths of the Gaussian defects as a function of light soaking time are presented in Figs. SI 3(a) and 3(b) in the supplementary material. These results obtained for the annealed states as well as for different light soaking intervals under well-controlled *in situ* light soaking and experimental conditions indicate that four different Gaussian-type midgap states located below the dark Fermi level were identified from the deconvolution of the α(hν) spectrum measured by the improved DBP method. It can be concluded from these results that the native and Staebler–Wronski defects created by light are the same types of defect distributions located at same energy positions. Extended light soaking causes only an increase in the total density of A, B, C, and X states at different rates in different time domains.

In order to correlate the changes in σ_{photo} measured under AM1.5 white light as well as that measured under the red light of the He–Ne laser shown in Fig. 14, the net changes in the total density of A, B, C, and X states are represented in Fig. 16 as a function of the light soaking time. At the lowest intensity of red light with a flux of 1×10^{13} cm^{-2} s^{-1}, the splitting of quasi-Fermi levels is so small that only the X and A states will contribute to the recombination of photocarriers. The total density of A and X states, $(N_A + N_X)$, increased linearly with a single exponent of $\beta = 0.10 \pm 0.02$ as shown in Fig. 16. Corresponding σ_{photo} measured at the flux of 1×10^{13} cm^{-2} s^{-1} degraded with a single power law of $t^{-\beta}$, where the exponent $\beta = 0.14 \pm 0.02$ in both regions indicates that changes in A and X states can be used to correlate with the changes in σ_{photo}. As the light intensity increases to 1×10^{15} cm^{-2} s^{-1} (medium light intensity), it is more likely that some portion or most of the B states will be covered by the quasi-Fermi levels and act as recombination centers for electrons. Time-dependent degradation of σ_{photo} at this medium intensity of

red light is expected to have a dependence on the total density of the A, B, and X states, $(N_A + N_B + N_X)$. In Fig. 16, this is presented as a function of the light soaking time, illustrating that $(N_A + N_B + N_X)$ increased with a single power law in both regions with the exponent $\beta = 0.18 \pm 0.02$. This is in good agreement with the fact that σ_{photo} measured at a flux of 1×10^{15} cm^{-2} s^{-1} degraded with a similar power law with the exponent $\beta = 0.20 \pm 0.02$ as shown in the inset of Fig. 14. Finally, at the highest intensity of AM1.5 white light, quasi-Fermi levels will extend to exponential valence and conduction band tails and C states will become efficient recombination centers. Thus, σ_{photo} (AM1.5) in both regions can be correlated with the net increase in the total density of A, B, C, and X states. In Fig. 16, the total density of Gaussians, $(N_A + N_B + N_C + N_X)$, is shown as a function of time. Two different time-dependent regions can be clearly identified. In region I, the total defect density increased slowly with time and can be fit to a power law of t^{β}, where $\beta = 0.10 \pm 0.02$, which is much lower than the degradation of σ_{photo} (AM1.5) in region I as shown in Fig. 14. It is more likely that at 1 sun intensity of AM1.5 white light, other defects located between the Fermi level and the conduction band edge acting as recombination centers are involved in the measured photoconductivity. Those defects cannot be probed by the DBP method. In region II, an increase in the total defect density of these four Gaussian defects showed a strong time dependence with a power law of t^{β}, where $\beta = 0.5 \pm 0.02$, mainly dominated by the increase in the C states as shown in Fig. 15(b). However, in region II, σ_{photo} (AM1.5) dominated by free electrons showed a much slower degradation with soaking time, tending to approach to a degraded steady-state. It can be understood from these results that the C states are inefficient recombination centers for electrons and more efficient recombination centers for free holes such that the degradation of p-i-n solar cells is mainly controlled by the C states under 1 sun operation as reported by Wronski *et al.*[19,22] It is more likely that the C states are non-D^0 states with negative charge since they must have very small capture cross sections for electrons and do not affect σ_{photo} (AM1.5).

VII. ROOM TEMPERATURE ANNEALING OF STAEBLER–WRONSKI DEFECTS

Recovery of solar cell efficiency at room temperature after high-intensity light soaking of a-Si:H solar cells introduced the concept of the "fast" and the "slow" states, for the first time, by Yang and Chen.[21] It was reported in that study that those states created faster anneal out easily even at room temperature. This effect was also investigated extensively in undoped a-Si:H films as a room temperature recovery of the photoconductivity or mobility-lifetime ($\mu\tau$) products of majority carriers after light soaking terminated and correlated with the recovery of dark forward-biased recombination currents in the intrinsic layers of p-i-n solar cells.[19,20,22,23,25,26,44] In the present study, room temperature annealing effects of the light-induced defects were also investigated by re-measuring the σ_{photo} and the $\alpha(h\nu)$ spectrum of the dc bias light-low1, a week after termination of light soaking. In Fig. 17, the raw Y_{DBP} spectra of the dc bias light-low1 are presented for the light-soaked state of 480 min measured right after and a week after light soaking. In the inset, the corresponding σ_{photo} of the sample

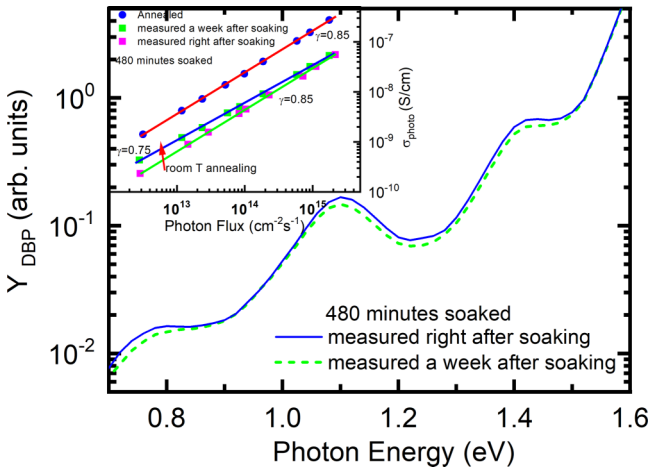

FIG. 17. Room temperature annealing of Staebler–Wronski defects as detected by the raw DBP spectra of the dc-bias light low1 measured right after and a week after light soaking of 480 min.

is shown together with that measured in the annealed state. There is a detectable decrease in the raw Y_{DBP} spectrum in the sub-bandgap energies below 1.5 eV for the measurement carried out a week after light soaking. This result indicates that the density of the electron-occupied midgap states below the dark Fermi level decreased a week after light soaking. It means that some portion of the defects below the Fermi level was annealed out at room temperature in dark. Similarly, a consistent improvement in photoconductivity, especially a more significant increase in the lower flux values, has been detected as seen in the inset of Fig. 17. The exponent γ of σ_{photo} on the flux was 0.85 in both annealed and light-soaked states as measured right after light soaking. However, the exponent γ decreased significantly to 0.75 for the measurement taken a week after light soaking and the values of σ_{photo} at lower flux values increased significantly as seen in the inset of Fig. 17. This can only be possible if the density of the midgap states acting as recombination centers located below the Fermi level decreases since the splitting of the quasi-Fermi levels is small at these low light intensities. At higher intensities of the measurement light, the recovery of σ_{photo} was found to be negligible. This recovery effect of σ_{photo} was attributed to room temperature annealing of the "fast" states created by light soaking.[21] However, the exact origin of the effect has not been understood until now. In order to examine the details of the observed effect, the σ_{photo} and $\alpha(h\nu)$ spectrum of the DBP dc bias light-low1 were re-measured a week after each light soaking period of degradations presented above. The Gaussian de-convolution of the recovered $\alpha(h\nu)$ spectrum was used to obtain the total density of A, B, C, and X states in the recovered state. The percent change in the density of each Gaussian distribution was calculated as $\%N_{DOS} = [100 \times (N_{right\ after} - N_{recovered})/N_{right\ after}]\%$. The corresponding percent increase in photoconductivity was calculated as $\%\sigma_{photo} = 100 \times [(\sigma_{photo}(\text{recovered}) - \sigma_{photo}\ (\text{right after soaking}))/\sigma_{photo}\ (\text{right after soaking})]\%$. The $\%\sigma_{photo}$ of the low flux, 1×10^{13} cm^2 s^{-1}, is presented above the "no-change line" and

that of $\%N_{DOS}$ is shown below the "no-change line" in Fig. 18. As the light soaking period increases, more recovery in σ_{photo} was recorded, indicating that more fast states are created as the soaking time increases and they anneal out at room temperature, making it more likely that annealing of the fast states takes place during light soaking. The defects responsible for this recovery of photoconductivity are presented below the "no-change line." It is clearly observed that there is no change in the density of C states for all light soaking periods. No significant room temperature annealing of the C states located closer to the valence band tails indicates that the C states with the highest density must be the "slow" states indicated in the literature.[19–23,25,26,44] Their annealing can only happen at higher temperatures above 150 °C as it is shown in Fig. 13. However, there are detectable changes in the total density of A, B, and X states, which decreased after a week of recovery. First of all, 6 min of light soaking indicated a very small recovery of σ_{photo}, about 10%. There was no detectable annealing in the density of A and X states, but only the density of B states decreased about 10%. As the light soaking time increases, the contribution of A and B states seemed to be constant, where the relative decrease in A states is found to be 15 ± 3% and that of B states is 12 ± 2%. However, for light soaking times longer than 20 min, room temperature annealing of X states becomes more significant in the recovery of photoconductivity. Since the X states are located in the middle of the bandgap, they are most efficient recombination centers for electrons. The percent change in the density of X states decreased almost linearly as the light soaking time increased, which finally contributed more to the large recovery of σ_{photo} as shown in Fig. 18. We can infer from these results that the X states could be the major component of the "fast" states created by light. The total

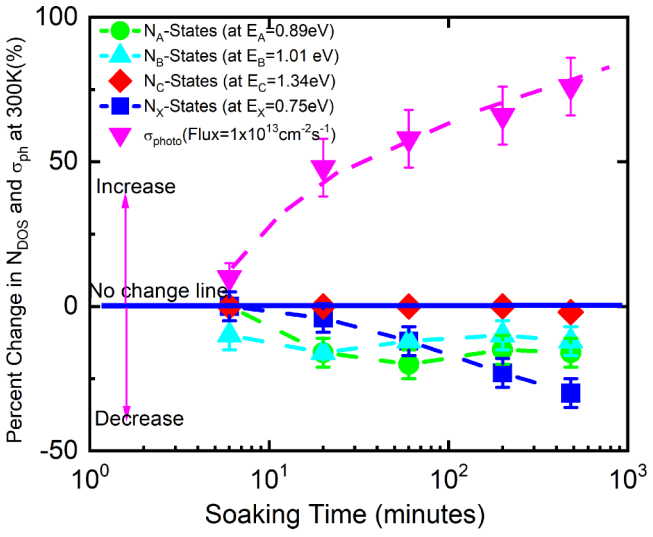

FIG. 18. Room temperature annealing of Staebler–Wronski defects as percent changes from the light-soaked values and corresponding percent improvement of steady-state photoconductivity measured a week after light soaking at 300 K. Lines are guide to eye.

percent decrease in A, B, and X states for the recovery of the 480 min light-soaked state is 57% as shown in Fig. 18. However, the percent increase in σ_{photo} for the recovery of the same light-soaked state was found to be 77%, indicating that in addition to the density of the occupied Gaussian defect states acting as recombination centers, their capture cross sections also play a role in determining this recovery process of photoconductivity. Such information about the capture cross sections of defect states can only be obtained by detailed numerical modeling of these results by taking into account all the defect states in the bandgap and their occupation statistics through the generation-recombination equations.[45]

VIII. DISCUSSION AND CONCLUSIONS

Photoconductivity methods are very sensitive to indirectly obtain very low levels of sub-bandgap absorption coefficients related to the occupied gap states located below the dark Fermi level of a-Si:H. In this section, we briefly discuss how the improved DBP method introduces new capabilities among the existing photoconductivity methods to determine the absolute α(hν) spectrum for the identification of multiple defects. The conventional DBP and CPM are not direct methods to get the α(hν) spectrum and require special data processing and normalization. First, interference fringes on the relative ac photoconductivity spectrum must be eliminated accurately. Second, the relative fringe-free photoconductivity spectrum must be normalized to the absolute α(hν) spectrum of the same sample obtained independently by transmittance/reflectance (T&R) or photothermal deflection spectroscopy (PDS) methods at single energy around the band edge where a sufficient overlap must exist between two spectra.[18,31,33] Alternatively, the absolute constant photocurrent method (A-CPM) was developed in 1995[46] by Vanecek *et al.* to obtain the fringe-free absolute α(hν) spectrum of a-Si:H. In this new approach, the measurements of transmission CPM and standard CPM spectra, after placing them in the absolute scale, were used to calculate the absolute fringe-free α(hν) spectrum together with the help of Ritter–Weiser optical equations.[38] In 2002, Vanecek and Poruba introduced a new method of photocurrent spectroscopy called Fourier transform photocurrent spectroscopy (FTPS) based on the work of Tomm *et al.*[47] to measure the α(hν) spectrum of thin silicon films as well as thin film silicon solar cells.[48] In FTPS, measured absorptance and transmission spectra were then used to calculate the fringe-free absolute α(hν) spectrum by using the Ritter–Weiser optical equations.[38] However, the measurement principles and data processing of the FTPS method involve many challenging problems in getting an accurate α(hν) spectrum as reported by Holovsky.[49] In addition, the relatively high intensity of white light used in the measurement of the complete α(hν) spectrum causes a substantial increase in the occupation of the defect states above the Fermi level and a corresponding increase in the calculated α(hν) spectrum in the sub-bandgap energies. Therefore, it is not possible to probe only the occupied defect states below the dark Fermi level by the FTPS method, i.e., the level for true occupied defect states in dark.

In this investigation, we have improved the conventional dual beam photoconductivity method[31] and applied it, for the first time, to study the Staebler–Wronski effect in undoped a-Si:H films by

obtaining a reliable and accurate fringe-free absolute α(hν) spectrum. In the improved DBP method, the relative ac photoconductivity spectra, Y_{DBP}, for different dc bias light intensities as well as the optical transmission spectrum, T, of the sample detected from the substrate side are measured simultaneously. Then, the fringe-free absolute α(hν) spectrum down to 0.66 eV was calculated by using the absolute Y_{DBP} and T spectra through Ritter–Weiser optical equations,[38] in analogy to A-CPM and FTPS methods. Modeling-based fringe removing procedures and normalization of the Y_{DBP} spectrum are not required. The calculated α(hν) spectrum was also compared with that independently measured by FTPS on the same sample and a very good overlap has been obtained from the visible region down to the exponential valence band tail energies as shown in Fig. 3. FTPS is powerful to obtain the α(hν) spectrum from 3.0 down to 0.6 eV, which was only possible in the past by using three different methods, i.e., spectroscopic ellipsometry, T&R, and DBP.[50] However, due to the relatively higher intensity of white light used in the FTIR spectrophotometer, a substantial increase exists in the calculated α(hν) spectrum in the sub-bandgap energies. This is shown for the high dc bias light DBP spectrum as presented in Fig. 2(a) as well as in Fig. 3 for the FTPS spectrum. For this reason, the lowest dc bias light DBP spectrum (dc bias light-low1) of the improved DBP is the key to study the density and energy distribution of the electron-occupied defect states located below the dark Fermi level in the annealed as well as in light-soaked states, after calculating the fringe-free absolute α(hν) spectrum.

The α(hν) spectrum is directly related to the imaginary part of the dielectric constant, ε_2, as defined by Eq. (1) if the spectral dependence of refractive index, n(hν), is available. It is generally known that the measurement of the n(hν) spectrum down to the sub-bandgap energies cannot be performed routinely for each sample due to experimental limitations. In our investigation, we have used the tenth-order polynomial fit function of n(hν) reported in the literature[36] to calculate the ε_2(hν) function of the sample for both DBP dc bias-low1 as well as the FTPS spectra. In the inset of Fig. 3, the $\varepsilon_2^{1/2}$ vs photon energy, which is known as the Cody plot, is presented for both DBP and FTPS measurements. It is clearly seen that the Cody plot of FTPS and improved DBP spectra obey perfectly to a straight line down to 1.90 eV, indicating optical transitions between the parabolic extended states. The Cody plot provided E_{CD} and ($N_{co}N_{vo}$) products of the sample, which are very valuable experimental data of the sample to calculate the theoretical joint density of states function, $J_{DOS}(h\nu) = J_{EE}(h\nu)$, which is defined for optical transitions between parabolic extended states for photon energies higher than E_{CD} as defined in Eq. (4), as well as to normalize the energy-dependent electron-occupied density of states function, kN_{gap}, in absolute scale. However, the J_{DOS} (hν) function below E_{CD}, corresponding to electron-occupied defect states located below the dark Fermi level, can only be obtained alternatively from the experimental α(hν) spectrum by using Eq. (3), if the spectral dependence of the refractive index, n(hν), as well as $R^2(h\nu)$, the average dipole matrix element squared, are known. It was shown in this work that the experimental $J_{DOS}(h\nu)$ down to the sub-bandgap energies was calculated by using the α(hν) spectrum of DBP dc bias light-low1 as well as that of the FTPS measurement and reported results for n(hν)[36] and $R^2(h\nu)$.[32] There is a perfect overlap between $J_{EE}(h\nu)$ and other $J_{DOS}(h\nu)$ functions down to E_{CD}, indicating that FTPS is powerful and fast to obtain optical transitions from electron-occupied parabolic valence band extended states to the empty parabolic conduction band extended states accurately, as compared with compatible optical methods of spectroscopic ellipsometry and T&R commonly used in the past to obtain the α(hν) spectrum corresponding to extended states.[50,51] Furthermore, there exists a perfect overlap between $J_{DBP}(h\nu)$ and $J_{FTPS}(h\nu)$ down to the bottom of exponential valence band tails. $J_{FTPS}(h\nu)$ is much higher in the sub-bandgap energy region due for two reasons: (1) it was measured after 1000 h of the light-soaked state at Delft University of Technology and (2) it was measured under a much higher intensity of measurement light. However, the $J_{DBP}(h\nu)$ spectrum obtained from dc bias light-low1 measurement corresponds to the distribution of electron-occupied midgap defect states located below the dark Fermi level. Therefore, the improved DBP method is powerful to study the density and energy locations of the native defects as well as the Staebler–Wronski defects created by light in undoped a-Si:H films.

In the annealed state, it was found that there are four distinctly different native defect states located below the Fermi level. These defects were named as A, B, C, and X states following the same previously used nomenclature.[13–15,28,29] They are located at photon energies of 0.89 ± 0.02, 1.0 ± 0.01, 1.34 ± 0.01, and 0.75 ± 0.02 eV, respectively, as shown in Fig. 6. The density of these Gaussian-type defects was found to be $(6.0 \pm 0.2) \times 10^{15}$, $(2.8 \pm 0.1) \times 10^{16}$, $(2.0 \pm 0.1) \times 10^{17}$, and $(4.0 \pm 0.1) \times 10^{15}$ cm^{-3} for A, B, C, and X states, respectively. Their half-widths are similar and vary within 120 ± 15 meV. The A, B, and C states were first identified by Wronski's group by using the conventional DBP method at photon energies of 0.85, 1.01, and 1.28 eV for A, B, and C states, respectively.[13–15] We have also tried to fit the kN_{gap} spectrum by using the peak energy positions of A, B, and C states reported by Wronski's group, but it was not possible to get an acceptable fit for the shape of the whole spectrum of kNgap due to the energy position of the X states located at 0.75 eV. The differences between conventional DBP and the improved DBP methods rely on the fringe removing process and the simultaneous measurement of optical transmission from exactly the same spot where ac photoconductivity is measured as well to obtain the absolute α(hν) spectrum. Conventional DBP used the Fourier transform methodology developed by Wiedeman *et al.*[52] for the fringe removing procedure, which might have introduced an artificial smoothing of natural fringes of DBP at lower photon energies such that X states might have been overlooked. However, in the improved DBP method, the fringes were removed naturally in optical equations used to calculate the absolute α(hν) spectrum[38] similarly carried out in the FTPS method.[14,15] The phase of the dc bias-light low1 shown in the insets of Figs. 2(a) and 8 indicates the accuracy of the measured response of the sample in the annealed and light-soaked states. The fourth Gaussian-type midgap state at photon energy around 0.70 eV was also reported for the first time by FTPS measurements carried out in similar quality undoped a-Si:H films as well as p-i-n solar cells.[14,15] These defects in the middle of the bandgap were named as X states since their origin and nature are unknown at the present, although it has been argued that they can be associated with doubly charged defect entities.[10,15] In this study, the X states

were also identified at a photon energy of 0.75 eV in addition to the other three defect states located at similar peak energy positions as consistent with recent FTPS measurements.[14,15]

In the light-soaked state, the density of these Gaussian-type defect states increased significantly by different rates as presented in Fig. 11 without any significant change in their peak energy positions and half-widths. It can be concluded that the native and Staebler–Wronski defects are the same type of defects present in the nanostructure of a-Si:H. Several sister samples from the same deposition run and with the same contact geometry were also studied in both annealed and light-soaked states. Those results are shown in Fig. SI 1 in the supplementary material indicating that four different Gaussian-type midgap defect states located below the dark Femi level were also identified in both annealed and light-soaked states at similar peak energy locations and half-widths, while only their density increased after light soaking.

Right after the discovery of the Staebler–Wronski effect, light-induced defects were thought to be paramagnetic neutral silicon dangling bonds, the D^o states.[2,3] However, it was reported several years ago that there exist two different paramagnetic silicon dangling bonds, D^o defects, in the nanostructure of undoped a-Si:H as detected by time-domain pulsed EPR spectroscopy.[16,17] These defects were named as Type I and Type II defect states. Type I defects are located at the inner surface of open volume deficiencies such as divacancy, multivacancy, and up to nanosized or microvoids, while Type II defects are isolated and randomly distributed silicon dangling bonds in the nanostructure of a-Si:H, which were the originally reported EPR defects.[2,3] Both types of paramagnetic defects were shown to be present in both annealed as well as light-soaked states. The majority of paramagnetic defects are randomly distributed silicon dangling bonds, labeled as Type II defects. It was shown that Type II defects make up 79% of the total paramagnetic defects and the rest, 21%, are Type I defects located on inner surfaces of microvoids.[16,17] These two types of paramagnetic silicon dangling bonds must be located below the dark Fermi level and detected by the sub-bandgap photoconductivity method of the improved DBP as well as by other photoconductivity methods such as FTPS and CPM. Therefore, two of the four Gaussian-type defect states identified by using the improved DBP method should correspond to the paramagnetic EPR defects of Type I and Type II. It is more likely that these defect states are A and B states located at the photon energy of 0.89 ± 0.05 and 1.0 ± 0.01 eV as presented above. The total density of N_A and N_B in the annealed state was found to be $N_{AB\text{-annealed}} = N_{A\text{-annealed}} + N_{B\text{-annealed}} = 3.4 \times 10^{16}\ cm^{-3}$. The ratio of $N_{B\text{-annealed}}/N_{AB\text{-annealed}}$ is 82% and that of $N_{A\text{-annealed}}/N_{AB\text{-annealed}}$ is 18%. In the light-soaked state, $N_{AB\text{-soaked}} = N_{A\text{-soaked}} + N_{B\text{-soaked}} = 1.12 \times 10^{17}\ cm^{-3}$. The ratio of $N_{B\text{-soaked}}/N_{AB\text{-soaked}}$ is 77% and that of $N_{A\text{-soaked}}/N_{AB\text{-soaked}}$ is 23%. These ratios of the density of A and B states to the total density obtained in annealed and light-soaked states are found to be in the similar range for the ratios of Type I and Type II defects to total paramagnetic defects. Therefore, our investigation supports that the A states could be the Type I and the B states could be Type II paramagnetic silicon dangling bond defects as reported by time-domain pulsed EPR spectroscopy.[16,17]

The other defects, the C and X states, are more likely related to the non-D^o defects that exist in the nanostructure of undoped a-Si:H. The effects of the non-D^o defects were reported extensively by Wronski's group and they play a major role in the degradation of $\mu\tau$-products of majority and minority carriers as well as in the degradation of p-i-n solar cells.[18–20] Specifically, C states closer to the valence band edge were shown to be efficient hole recombination centers and responsible for the degradation of solar cells under 1 sun illumination.[53,54] The C states must be the negatively charged non-D^0 states since they do not degrade σ_{photo} (AM1.5) significantly after 2 h of extended light soaking, even if their density increases strongly with time. It was reported that the nanostructure of dense a-Si:H is well described by an anisotropic disordered network in which a high density of hydrogenated divacancies exists,[8–10] which was also confirmed by several investigations that hydrogen passivated divacancies are the dominant sites in dense a-Si:H.[55–58] In the anisotropic disordered network, the not fully hydrogenated divacancy will result in multiple defect states in the bandgap of a-Si:H, including the paramagnetic D^o states like Type I and Type II defects as well as the non-D^o defects-like charged defects. However, no theoretical modeling has been carried out to calculate the energy locations of such multiple defects yet. Our experimental results clearly indicate that some of these multiple defects below the Fermi level are located at photon energies indicated above and are detected by the improved DBP method.

In addition to the presence of multiple defects in the nanostructure of a-Si.H, their kinetics under light has also been an important investigation. It was first theoretically demonstrated by Stutzmann, Jackson, and Tsai (SJT) in 1985, who argued that the light-induced defects are created by recombination of free carriers under light and their kinetics was shown to be proportional to $G^{2/3} t^{1/3}$, where G stands for the generation rate of light and t is light soaking time.[4] In 1998, Branz proposed an alternative theoretical approach to explain the Staebler–Wronski effect and its kinetics in a-Si:H through the hydrogen collision process taking place during light soaking.[6,7] The kinetics of the light-induced defect creation on light intensity and time was also predicted as proportional to $G^{2/3} t^{1/3}$, the same as that of the SJT model even though these two models were based on different physical origins. These two theoretical models assumed the same isolated silicon dangling bonds as the main defect, i.e., single electron-occupied neutral silicon dangling bonds, D^o states, as well as hydrogen atoms randomly distributed in the continuous random network. However, it was recently reported in 2014 by Fehr *et al.* that there are two types of neutral silicon dangling bonds, paramagnetic D^o states, in the nanostructure of undoped a-Si:H, labeled as Type I and Type II defects by using time-domain pulsed EPR experiments.[16] Both Type I and Type II defects were shown to play a major role in the Staebler–Wronski effect.[16] Therefore, a single kinetics rate equation as proposed by the SJT[4] and hydrogen collision models[6,7] cannot explain the kinetics of the light-induced defect creation and the corresponding degradation of photoconductivity in undoped a-Si:H; as has also been experimentally demonstrated through the FTPS analysis.[14] It was also reported that the kinetics of the Staebler–Wronski effect depends on the initial defect density present before light soaking as well as the sample temperature.[14,18,19,22] Therefore, studying the kinetics of light-induced defects requires well-defined experimental conditions before and after light soaking for a reliable comparison of experimental results among different laboratories as

well as among the different samples in the same laboratory. For this reason, we have applied a single-step light soaking of undoped a-Si:H films at a constant temperature in a well-controlled soaking ambient of high vacuum under 1 sun and from the same reproducible annealed state defect densities as presented in Figs. 12 and 13. Evolution of four different Gaussian defect states was obtained as a function of the light soaking time and correlated with measured photoconductivity and the $\alpha(h\nu)$ spectrum. It was found that two different time regions exist in defect creation as reported by Wronski *et al.*[22,29] Within 120 min of light soaking, the net density of A, B, C, and X states is almost constant at certain values and show no significant time dependence. For light soaking longer than 120 min, the net increase in the density of the X states is almost independent of the light soaking time and stays constant at $4 \pm 0.5 \times 10^{15}\,cm^{-3}$ within the experimental error. The A states increase very slowly with the exponent $\beta = 0.1 \pm 0.02$. However, the net increase in the density of B and C states shows a stronger time dependence and obey t^{β}, where the exponent $\beta = 0.5 \pm 0.02$. Corresponding net changes in the densities of A, B, C, and X states can be partially correlated with net changes in the $\alpha(h\nu)$ measured at the peak energy positions of A, B, C, and X states as presented in Figs. 15(a) and 15(b). However, it is not possible to make one-to-one correlations with the decrease in σ_{photo} measured at low and medium intensities of red light as well as at AM1.5 intensity as shown in Fig. 14 with the kinetics of a single Gaussian defect presented in Fig. 15(b).[18,19,59]

Finally, it was also important to discuss the room temperature annealing of light-induced defects occurring right after termination of light soaking as first reported by Yang and Chen.[21] The concept of the "fast" and the "slow" states defined in that study also brings about difficulties in the investigation of light-induced defect kinetics. It was found in this study that there was a significant recovery in σ_{photo} of the light-soaked state as measured approximately a week after light soaking. Room temperature recovery of σ_{photo} measured at the low intensity of red light is mainly due to annealing of A, B, and X states located closer to the middle of the bandgap, which define the "fast" states. The C states do not show any detectable annealing effect suggesting that they must represent the "slow" states as defined in the literature.[21–26]

In conclusion, more than four decades after its discovery, we have improved the original dual beam photoconductivity method of Wronski and his collegues[31] and applied it to study the Staebler–Wronski effect in dense undoped a-Si:H films. In addition to the three Gaussian-type midgap defect states previously reported by Wronski's group[28] by using the conventional DBP method, we have identified the fourth Gaussian-type midgap state in the annealed state just at the middle of the bandgap at a photon energy of 0.75 eV by using the improved DBP method, as consistent with the results obtained by FTPS. In the light-soaked state, these four different Gaussian-type defects appear at same photon energy positions and with similar half-widths of native defects, so only an increase in their density defines the SWE. Two of these four defects, A and B states, could possibly be representing the recently discovered Type I and Type II paramagnetic EPR defects by Fehr *et al.*[16] Other C and X states could be representing the non-D^o states, i.e., charged defects present in the nanostructure of undoped a-Si:H. Such multiple defect states in the nanostructure of a-Si:H were projected only by the anisotropic disordered network model, where the not fully hydrogenated divacancy could result in multiple native and light-induced defects. However, the theoretical model calculations for the energy locations of such multiple defects are missing in the literature and are extremely important to understand the four-decades-old problem of the Staebler–Wronski effect. It was also found that the kinetics of the light-induced defect creation cannot simply be defined by a single rate equation, since each defect distribution has a different time rate under light and contributes differently to the degradation of photoconductivity measured at different generation rates. Furthermore, the results obtained in this study indicate that three of these Gaussian-type defect states located closer to the middle of the bandgap, the A, B, and X states, are more likely the "fast" states and the C states located closer to the valence band edge are the "slow" states.

SUPPLEMANTARY MATERIAL

See the supplementary material for the data cited in the text.

ACKNOWLEDGMENTS

This paper is dedicated to the late Professor Christopher R. Wronski who contributed to the discovery of the Staebler–Wronski effect in a-Si:H, to the invention of the first a-Si:H p-i-n solar cell, and to the development of amorphous silicon solar cell technology. The authors would like to thank Professor S. K. O'Leary for kindly providing the tenth order polynomial fit function to the refractive index spectrum of a-Si:H. Finally, we acknowledge Y. Mohammadian of Delft University of Technology for assistance in conducting the FTPS measurements and the corresponding spectral data analysis. We acknowledge financial support for this research from ADEM, A green Deal in Energy Materials of the Ministry of Economic Affairs of The Netherlands (www.adem-innovationlab.nl) and the STW Vidi project of A.H.M. Smets from Delft University of Technology.

AUTHOR DECLARATIONS

Conflict of Interest

The authors have no conflicts to disclose.

Author Contributions

Mehmet Güneş: Investigation (equal); Writing – original draft (equal); Writing – review & editing (equal). **Jimmy Melskens:** Investigation (equal); Writing – original draft (equal); Writing – review & editing (equal). **Arno H. M. Smets:** Investigation (equal); Writing – original draft (equal); Writing – review & editing (equal).

DATA AVAILABILITY

The data that support the findings of this study are available within the article and its supplementary material.

REFERENCES

[1]D. L. Staebler and C. R. Wronski, Appl. Phys. Lett. **31**, 292–294 (1977).
[2]H. Dersh, J. Stuke, and J. Beichler, Appl. Phys. Lett. **38**, 456–458 (1981).

[3]R. E. Street, D. K. Biegelsen, and J. C. Knights, Phys. Rev. B **24**, 969–984 (1981).
[4]M. Stutzmann, W. B. Jackson, and C. C. Tsai, Phys. Rev. B **32**, 23–47 (1985).
[5]M. J. Powell and S. C. Deane, Phys. Rev. B **48**, 10815–10827 (1993).
[6]H. M. Branz, MRS Proc. **507**, 709 (1998).
[7]H. M. Branz, Phys. Rev. B **59**, 5498–5512 (1999).
[8]A. H. M. Smets, W. M. M. Kessels, and M. C. M. van Sanden, Appl. Phys. Lett. **82**, 1547–1549 (2003).
[9]A. H. M. Smets and M. C. M. van de Sanden, Phys. Rev. B **76**, 073202 (2007).
[10]A. H. M. Smets, C. R. Wronski, M. Zeman, and C. M. van de Sanden, MRS Proc. **1245**, A1402 (2010).
[11]J. Melskens, S. W. H. Eijt, M. Schouten, A. S. Vullers, A. Mannheim, H. Schut, B. Macco, M. Zeman, and A. H. M. Smets, IEEE J. Photovoltaics **7**, 421–429 (2017).
[12]J. Melskens, A. H. M. Smets, S. W. H. Eijt, H. Schut, E. Brück, and M. Zeman, J. Non-Cryst. Solids **358**, 2015–2018 (2012).
[13]J. Melskens, A. H. M. Smets, M. Schouten, S. W. H. Eijt, H. Schut, and M. Zeman, IEEE J. Photovoltaics **3**, 65–71 (2013).
[14]J. Melskens, M. Schouten, A. Mannheim, A. S. Vullers, Y. Mohammadian, S. W. H. Eijt, H. Schut, T. Matsui, M. Zeman, and A. H. M. Smets, IEEE J. Photovoltaics **4**, 1331–1336 (2014).
[15]J. Melskens, M. Schouten, R. Santbergen, M. Fischer, R. Vasudevan, M. Zeman, and A. H. M. Smets, Sol. Energy Mater. Sol. Cells **129**, 70–81 (2014).
[16]M. Fehr, A. Schnegg, B. Rech, O. Astakhov, F. Finger, R. Bittl, C. Teutloff, and K. Lips, Phys. Rev. Lett. **112**, 066403 (2014).
[17]J. Melskens, A. Schnegg, A. Baldansuren, K. Lips, M. P. Plokker, S. W. H. Eijt, H. Schut, M. Fischer, M. Zeman, and A. H. M. Smets, Phys. Rev. B **91**, 245207 (2015).
[18]M. Güneş and C. R. Wronski, J. Appl. Phys. **81**, 3526–3536 (1997).
[19]J. Pearce, X. Niu, R. Koval, G. Ganguly, D. Carlson, R. W. Collins, and C. R. Wronski, MRS Proc. **664**, A1231 (2001).
[20]J. M. Pearce, J. Deng, V. Vlahos, R. W. Collins, C. R. Wronski, J. Whitaker, and P. C. Taylor, MRS Proc. **808**, A2.5 (2004).
[21]L. Yang and L. Chen, Appl. Phys. Lett. **63**, 400–402 (1993).
[22]C. R. Wronski, J. M. Pearce, R. J. Koval, X. Niu, A. S. Ferlauto, J. Koh, and R. W. Collins, MRS Proc. **715**, A13.4 (2002).
[23]J. M. Pearce, R. J. Koval, X. Niu, S. J. May, R. W. Collins, and C. R. Wronski, in *17th European Photovoltaic Solar Energy Conference Proceedings* (EU PVSEC, 2002),Vol. 3, p. 2842.
[24]M. L. Albert, J. Deng, X. Niu, J. M. Pearce, R. W. Collins, and C. R. Wronski, MRS Proc. **862**, A13.2.1 (2005).
[25]J. M. Pearce, J. Deng, M. L. Albert, C. R. Wronski, and R. W. Collins, in *Conference Record of the IEEE Photovoltaic Specialists Conference* (IEEE, 2005), pp. 1536–1539.
[26]J. Deng, J. M. Pearce, V. Vlahos, R. W. Collins, and C. R. Wronski, MRS Proc. **808**, 623–628 (2004).
[27]R. Vasudevan, I. Poli, D. Deligiannis, M. Zeman, and A. H. M. Smets, IEEE J. Photovoltaics **7**, 656–664 (2017).
[28]L. Jiao and C. R. Wronski, MRS Proc. **1066**, 99–104 (2008).
[29]C. R. Wronski and X. Niu, IEEE J. Photovoltaics **4**, 778–784 (2014).
[30]M. Vanecek, J. Kocka, J. Stuchlik, and A. Triska, Solid State Commun. **39**, 1199–1202 (1981).
[31]S. Lee, S. Kumar, C. R. Wronski, and N. Maley, J. Non-Cryst. Solids **114**, 316–318 (1989).
[32]W. B. Jackson, S. M. Kelso, C. C. Tsai, J. W. Allen, and S.-J. Oh, Phys. Rev. B **31**, 5187–5198 (1985).
[33]L. Jiao, I. Chen, R. W. Collins, C. R. Wronski, and N. Hata, Appl. Phys. Lett. **72**, 1057–1059 (1998).
[34]S. M. Malik and S. K. O'Leary, Appl. Phys. Lett. **80**, 790–792 (2002).
[35]S. K. O'Leary and S. M. Malik, J. Appl. Phys. **92**, 4276–4282 (2002).
[36]J. J. Thevaril and S. K. O'Leary, J. Appl. Phys. **120**, 135706 (2016).
[37]R. H. Klazes, M. H. L. M. van den Broek, J. Bezemer, and S. Radelaar, Philos. Mag. B **45**, 377–383 (1982).
[38]D. Ritter and K. Weiser, Opt. Commun. **57**, 336–338 (1986).
[39]G. D. Cody, T. Tiedje, B. Abeles, B. Brooks, and Y. Goldstein, Phys. Rev. Lett. **47**, 1480–1483 (1981).
[40]J. M. Pearce, J. Deng, R. W. Collins, and C. R. Wronski, Appl. Phys. Lett. **83**, 3725–3727 (2003).
[41]M. Güneş, D. Akdaş, O. Göktaş, R. Carius, J. Klomfass, and F. Finger, J. Mater. Sci. Mater. Electron. **14**, 729–730 (2003).
[42]M. Güneş, C. R. Wronski, and T. J. McMahon, J. Appl. Phys. **76**, 2260–2263 (1994).
[43]N. Wyrsch, F. Finger, T. J. McMahon, and M. Vanecek, J. Non-Cryst. Solids **137–138**, 347–350 (1991).
[44]M. L. Albert, J. Deng, X. Niu, J. M. Pearce, R. W. Collins, and C. R. Wronski, MRS Proc. **862**, 457–462 (2005).
[45]J. G. Simmons and G. W. Taylor, Phys. Rev. B **4**, 502–511 (1971).
[46]M. Vanecek, J. Kocka, A. Poruba, and A. Fejfar, J. Appl. Phys. **78**, 6203–6210 (1995).
[47]J. W. Tomm, A. Jaeger, A. Bärwolff, and T. Elsaesser, Appl. Phys. Lett. **71**, 2233–2235 (1997).
[48]M. Vanecek and A. Poruba, Appl. Phys. Lett. **80**, 719–721 (2002).
[49]J. Holovský, "Fourier transforms—New analytical approaches and FTIR strategies," in *inTech.*, edited by G. Nikolić (IntechOpen, 2011), pp. 257–282, see http://www.intechopen.com/books/fourier-transforms-new-analytical-approaches-and-ftir-strategies/fourier-transform-photocurrent-spectroscopy-on-non-crystalline-semiconductors
[50]A. S. Ferlauto, G. M. Ferreira, J. M. Pearce, C. R. Wronski, and R. W. Collins, J. Appl. Phys. **92**, 2424–2436 (2002).
[51]Y. Lu, I. An, M. Günes, M. Wakagi, C. R. Wronski, and R. W. Collins, Appl. Phys. Lett. **63**, 2228–2230 (1993).
[52]S. Wiedeman, M. S. Bennett, and J. L. Newton, MRS Proc. **95**, 145 (1987).
[53]C. R. Wronski, J. Deng, X. Niu, and A. H. M. Smets, in *IEEE 35th Photovoltaic Specialists Conference* (IEEE, 2010), Vol. 1, p. 146.
[54]J. Deng, B. Rross, M. Albert, R. W. Collins, and C. R. Wronski, MRS Proc. **910**, A0202 (2006).
[55]J. Baum, K. K. Gleason, A. Pines, A. N. Garroway, and J. A. Reimer, Phys. Rev. Lett. **56**, 1377–1380 (1986).
[56]Z. Remeš, M. Vaněček, A. H. Mahan, and R. S. Crandall, Phys. Rev. B **56**, R12710–R12713 (1997).
[57]R. Suzuki, Y. Kobayashi, T. Mikado, A. Matsuda, P. J. Mcelheny, S. Mashima, H. Ohgaki, M. Chiwaki, T. Yamazaki, and T. Tomimasu, Jap. J. of Appl. Phys. **30**, 2438 (1991).
[58]J. T. Stephen, J. M. Rutland, D. Dan, and Y. Wu, MRS Proc. **467**, 159 (1997).
[59]R. Koval, X. Niu, J. Pearce, L. Jiao, G. Ganguly, J. Yang, S. Guha, R. W. Collins, and C. R. Wronski, MRS Proc. **609**, A15.5 (2000).